Tectonophysics 609 (2013) 504–523

Contents lists available at ScienceDirect

Tectonophysics

journal homepage: www.elsevier.com/locate/tecto

Review Article

Earthquake cycle deformation and the Moho: Implications for the rheology of continental lithosphere

Tim J. Wright [a,*], John R. Elliott [b], Hua Wang [c], Isabelle Ryder [d]

[a] COMET +, School of Earth and Environment, University of Leeds, Leeds LS2 9JT, UK
[b] COMET +, Department of Earth Sciences, University of Oxford, Oxford OX1 3AN, UK
[c] Department of Surveying Engineering, Guangdong University of Technology, Guangzhou, China
[d] School of Environmental Sciences, 4 Brownlow St, University of Liverpool, L69 3GP, UK

ARTICLE INFO

Article history:
Received 18 June 2012
Received in revised form 20 July 2013
Accepted 22 July 2013
Available online 6 August 2013

Keywords:
Moho
Crustal deformation
Geodesy
Continental rheology
Elastic thickness

ABSTRACT

The last 20 years has seen a dramatic improvement in the quantity and quality of geodetic measurements of the earthquake loading cycle. In this paper we compile and review these observations and test whether crustal thickness exerts any control. We found 78 earthquake source mechanisms for continental earthquakes derived from satellite geodesy, 187 estimates of interseismic "locking depth", and 23 earthquakes (or sequences) for which postseismic deformation has been observed. Globally we estimate seismogenic thickness to be 14 ± 5 and 14 ± 7 km from coseismic and interseismic observations respectively. We find that there is no global relationship between Moho depth and the seismogenic layer thickness determined geodetically. We also found no clear global relationship between seismogenic thickness and proxies for the temperature structure of the crust. This suggests that the effect of temperature, so clear in oceanic lithosphere, is masked in the continents by considerable variation in lithology, strain-rate, and/or grain size. Elastic thicknesses from Bouguer gravity are systematically larger than the geodetic seismogenic thicknesses but there is no correlation between them. By contrast, elastic thicknesses from free-air methods are typically smaller than the geodetic estimates of seismogenic layer thickness. Postseismic observations show considerable regional variations, but most long-term studies of large earthquakes infer viscoelastic relaxation in the lower crust and/or upper mantle with relaxation times of a few months to a few hundred years. These are in apparent contradiction with the higher estimates of elastic thickness. Our analysis of the geodetic data therefore supports the "crème brûlée" model, in which the strength of the continental lithosphere is predominantly in the upper seismogenic layer. However, the distribution of geodetic observations is biased towards weaker areas, and faults can also modify the local rheology. Postseismic results could therefore be sampling weak regions within an otherwise strong crust or mantle.

Contents

* Corresponding author. Tel.: +44 113 3435258.
E-mail address: t.j.wright@leeds.ac.uk (T.J. Wright).

0040-1951/$ – see front matter © 2013 Elsevier B.V. All rights reserved.
http://dx.doi.org/10.1016/j.tecto.2013.07.029

1. Introduction

The earthquake deformation cycle is typically divided into three phases: The deformation that occurs during an earthquake is referred to as *coseismic*; it is followed by a period of transient *postseismic* deformation, which eventually decays to a steady-state background *interseismic* deformation (e.g. Thatcher and Rundle, 1979). Recent advances in satellite geodesy, and in particular the rapid uptake of interferometric synthetic aperture radar (InSAR), have led to a dramatic increase in the quantity and quality of deformation measurements of the earthquake cycle (e.g. Bürgmann and Dresen, 2008; Weston et al., 2012; Wright, 2002).

Owing to the long inter-event time in many fault zones, typically hundreds to thousands of years, we do not have deformation observations with modern instruments spanning a complete earthquake cycle for any single fault. Nevertheless, by looking globally we can observe deformation around faults at different stages of the cycle. InSAR is particularly suitable for measuring the large and rapid coseismic displacements associated with continental earthquakes, but has also been valuable in constraining postseismic and interseismic deformation in several cases, particularly for remote faults with minimal ground-based observations. At the same time, thousands of Global Positioning System (GPS) measurements have been made in active fault zones (e.g. Kreemer et al., 2003). These have been particularly valuable for examining the slower, longer-wavelength deformation associated with the interseismic and postseismic phases of the earthquake cycle.

In the past decade, the strength of continental lithosphere has been the cause for considerable controversy (e.g. Bürgmann and Dresen, 2008; Burov, 2010; Burov and Watts, 2006; Jackson, 2002; Jackson et al., 2008). The debate has focused on whether strength resides in a single layer in the upper crust (the "crème brûlée" model) or whether the upper mantle is also strong (the "jelly sandwich" model). Most earthquakes occur in the upper crust; coseismic deformation can be used to infer the depth range of faulting and hence the thickness of the seismogenic layer. During the interseismic and postseismic periods, deformation occurs in the lower crust and mantle. We can infer the seismogenic thickness from simple elastic models of the interseismic period; the rates, location and mechanisms of postseismic deformation can be used to place bounds on the strength of the lower crust and upper mantle.

In this paper, we compile observations of earthquake cycle deformation from the published literature made in tectonic areas across the planet, and extract key parameters. In particular we examine the thickness of the upper crustal layer that slips in earthquakes but is locked in the interseismic period, and examine the depth ranges and timescales over which postseismic relaxation has been inferred to occur. We test whether these parameters are related to estimates of Moho depth, elastic thickness, and geothermal gradient, estimated independently. Finally, we discuss the implications for the strength of continental lithosphere.

2. Seismogenic thickness constraints from coseismic deformation

During coseismic deformation, the passage of seismic waves through the entire crust and mantle is testament to their elastic behaviour on short time-scales. On longer timescales, elastic stresses are relaxed through temperature-dependent ductile processes such as viscous relaxation (e.g. Pollitz, 1992; Rundle and Jackson, 1977) and aseismic afterslip (e.g. Perfettini and Avouac, 2004; Scholz and Bilham, 1991). These processes restrict the vast majority of continental earthquakes to the brittle upper crust. The thickness of this seismogenic layer (T_s) has previously been estimated by examining earthquake centroid depths (e.g. Jackson et al., 2008; Maggi et al., 2000) determined by inversions of seismic waves that assume a point source for the earthquake. Geodetic methods allow for additional information about the depth distribution of slip in earthquakes. For small events, most studies assume uniform slip on a rectangular dislocation (Okada, 1985). For larger events, detailed slip distributions are often resolved. In most of these cases, information about the maximum depth extent of slip in the earthquake can be retrieved. Although there are fewer geodetic earthquake solutions than seismic sources, the depth range over which seismic slip occurs is arguably more robust.

We have updated the list of 58 continental earthquakes ($Mw \gtrsim 5.5$) studied with InSAR from Weston et al. (2011, 2012), with 20 further earthquakes, to give a database of 78 events (Fig. 1a). The list is spread slightly unevenly across strike-slip (Table 1), normal (Table 2) and reverse (Table 3) faulting mechanisms, with 32, 21 and 25 events respectively. For each earthquake we extract the bottom depth of faulting in the published geodetic model.

The majority of studies involve models in which slip is permitted to occur over a distributed region of sub-fault patches. A limitation of surface geodetic data is that the resolution of slip decreases with depth (e.g. Atzori and Antonioli, 2011; Funning et al., 2005b) and that, consequently, small deep earthquakes are difficult to record. However, of the 78 continental earthquakes so far measured, the depth extent of faulting is clustered in the depth range 5–25 km, and slip much deeper than this has been shown to be recoverable for subduction events (e.g. Pritchard et al., 2002). The spread of InSAR bottom depths of faulting is normally distributed with a mean of 14 km and a standard deviation of 5 km (Fig. 2 inset). The depth distribution of smaller events, which are unlikely to have ruptured the entire width of the seismogenic crust, is biased towards the shallower range of depths in our database as they are difficult to detect geodetically if they occur in the mid-lower crust.

We compare the depth estimates of faulting from InSAR with seismic source models (Tables 1–3; Fig. 2), where available (86% of events examined here). To ensure the seismic solutions are robust and reliable, we only use centroid depths from point-source body-wave modelling (typically for smaller events) and distributed slip source models from body-wave/strong motion (for the larger events). For the larger events, we take the bottom depth of faulting in the slip model presented by the authors in each paper, as was done for the InSAR solutions. For the earthquakes with distributed seismic solutions, (circles in Fig. 2), there is a one-to-one correlation between the two estimates of bottom depth, with a small bias of 2–3 km towards deeper seismological slip when compared to the bottom depth from InSAR. This slight discrepancy may arise from the poorer depth resolution in the seismological solutions, or be because the InSAR models (which typically use homogeneous elastic half-spaces) bias the slip slightly shallower compared to the layered velocity models typically used in the seismology inversions. When the InSAR depths are compared to the seismological centroid depths (squares in Fig. 2), the relationship follows a two-to-one ratio, as would be expected if the slip was symmetrically distributed about the centroid in depth and approached the surface.

We compare the geodetically-determined bottom depth of rupture given in Tables 1–3 to the crustal thickness from Crust 2.0 (Bassin et al., 2000), for each type of fault mechanism (Fig. 3). The maximum depth of slip for the earthquakes with geodetic solutions is mostly in the range of 5–25 km, and occurs in regions with crustal thickness in the range of 10–75 km. There is a large spread in the data, but we find no systematic relationship between a deeper Moho and the depth extent of faulting.

3. Seismogenic thickness constraints from interseismic deformation

Simple geodynamic models of the entire earthquake cycle, with an elastic lid overlying a viscoelastic (Maxwell) substrate, suggest that the observed deformation is a function of time since the last earthquake (e.g. Savage, 1990; Savage and Prescott, 1978). Observations of focused strain late in the earthquake cycle around many major fault structures and rapid postseismic transients cannot be explained by these simple models — the former requires a high viscosity in the substrate and the latter a low viscosity (e.g. Hetland and Hager, 2006; Takeuchi and Fialko, 2012).

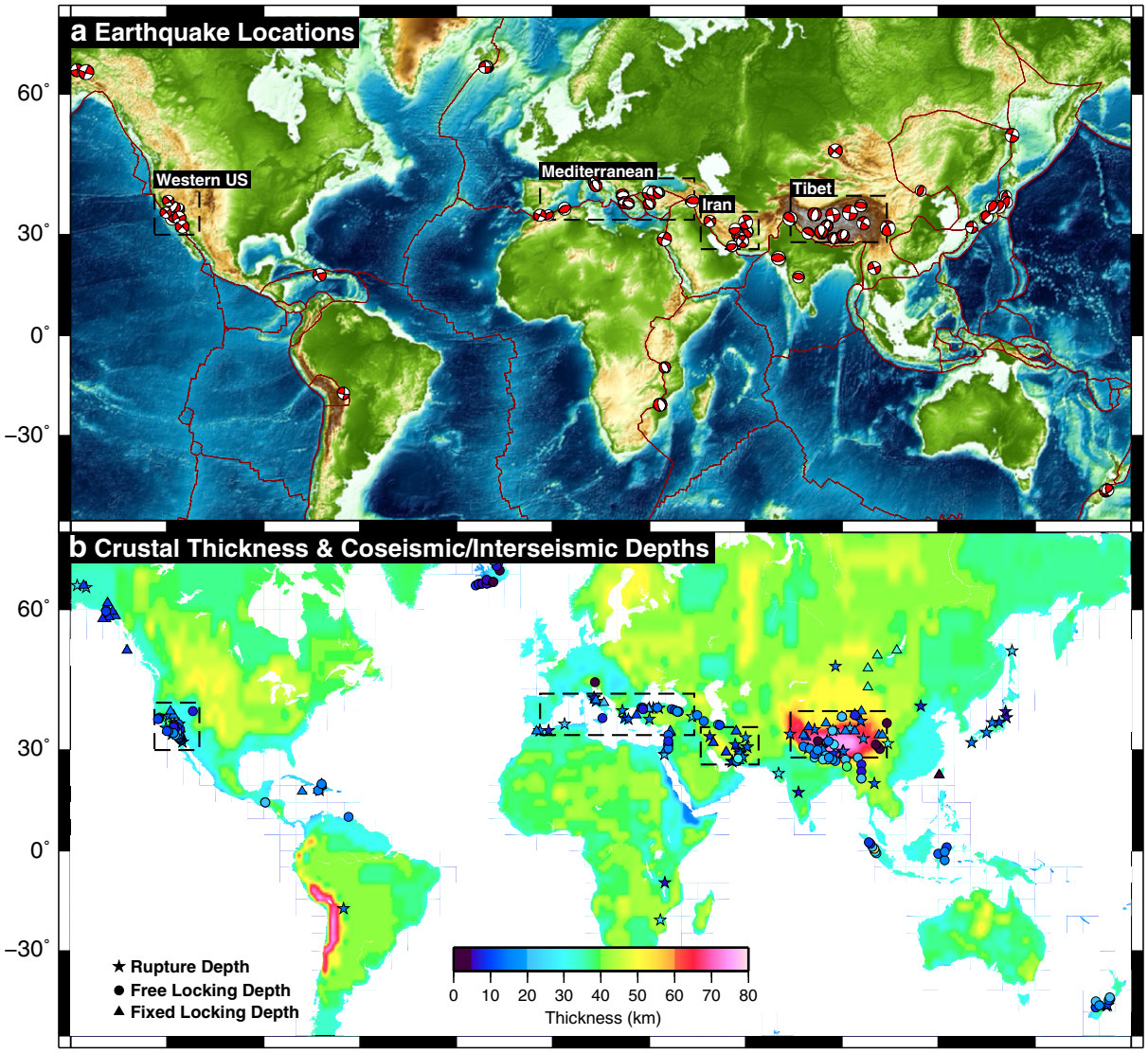

Fig. 1. (a) Locations and focal mechanisms of the 78 continental M_w 5.5 + earthquakes modelled to date with InSAR observations of surface deformation, updated from Weston et al. (2011, 2012) and listed in Tables 1–3. The areas of four continental regions used to subdivide the plots in Fig. 5 are delineated by dashed lines. (b) Crustal thickness from Crust 2.0 (Bassin et al., 2000), linearly interpolated to one degree spacing. Coloured stars indicate the bottom depth of faulting from coseismic studies (Tables 1–3). Locations of interseismic studies listed in Table 4 are coloured by depth and denoted by triangles (fixed locking depths) and circles (estimated locking depths).

The observational data have led to the development of a new generation of earthquake cycle models that are able to predict focused interseismic deformation alongside rapid postseismic deformation (Hetland and Hager, 2006; Johnson et al., 2007; Takeuchi and Fialko, 2012; Vaghri and Hearn, 2012; Yamasaki et al., 2013). These studies suggest that, although the velocities do change throughout the cycle, they are reasonably steady after the initial postseismic transient deformation has decayed. The models partially explain the ubiquity of the classic elastic dislocation model (Savage and Burford, 1973), in which interseismic deformation around strike-slip faults is modelled as steady creep on a narrow, infinitely-long and deep vertical fault in an elastic half space beneath a locked lid (the other significant factor is its simplicity).

We take a pragmatic approach to interseismic deformation, and have searched for all examples that have been modelled either using the simple deep dislocation formulation or an equivalent elastic block model approach. This allows us to examine spatial variations in the 'locking depth' parameter in a consistent manner, even if the model is undoubtedly an oversimplification.

We found 187 estimates of interseismic locking depth in ~100 publications (Table 4; Fig. 1). Of these, 131 were determined as free parameters in inversions of the geodetic data. Regional variations do exist, with locking depths in Iceland being 7 ± 4 km, compared with 20 ± 6 km in the Himalayas, for example. However, in general the values are remarkably consistent, normally distributed with a global mean of 14 ± 7 km (Fig. 4). This is remarkably similar to the global distribution found for the coseismic bottom depths (Fig. 2), with the same mean at 14 km. As was the case for earthquake depths, we find no systematic global relationship between locking depth and crustal thickness (Fig. 4).

4. Regional variations in seismogenic thickness

To search for any systematic variations in seismogenic thickness, we examine the distribution of coseismic slip and interseismic locking depths in four continental areas for which we have a sufficient number of geodetic results: Iran, the Mediterranean, Tibet and the Western US (Fig. 5).

For Iran, the 11 earthquakes so far studied are constrained to be shallower than 20 km and match the interseismic locking depths except for two deep outliers (Fig. 5). The results indicate a large aseismic lower crust above the Moho, which is at a depth of 40–45 km.

The Mediterranean region, which we define broadly to include 16 earthquakes in Turkey, Greece, Italy and Algeria, has depths of faulting

Table 1
Compilation of continental strike-slip earthquakes studied with InSAR, updated from Weston et al. (2011, 2012) to include the bottom depth of faulting (D) and more recent InSAR constrained source models. The type of model used is denoted by uniform (U) or distributed (D) slip. Seismological source model depths (Z) are given where available as centroid depths for point sources or bottom depths for finite fault planes, the latter denoted by an asterisk.

#	Name	M_w	Date	Lat.	Lon.	D (km)	Slip	Reference	Z (km)	Reference
1	Landers, CA., USA	7.3	1992/06/28	34.45	243.48	15	D	Fialko (2004b)	15*	Wald and Heaton (1994)
2	Al Hoceima, Morocco	6.0	1994/05/26	35.20	355.94	12	U	Biggs et al. (2006)	8	Biggs et al. (2006)
3	Double Spring Flat, NV., USA	6.0	1994/09/12	38.82	240.38	12	U	Amelung and Bell (2003)	6	Ichinose et al. (1998)
4	Kobe, Japan	6.9	1995/01/17	34.62	135.06	15	U	Ozawa et al. (1997)	20*	Ide et al. (1996)
5	Neftegorsk, Sakhalin, Russia	7.2	1995/05/27	52.89	142.90	22	U	Tobita et al. (1998)	9	Katsumata et al. (2004)
6	Nuweiba, Egypt	7.3	1995/11/22	28.88	34.75	20	D	Baer et al. (2008)	15	Hofstetter et al. (2003)
7	Kagoshima-kenhokuseibu, Japan	6.1	1997/03/26	31.98	130.40	14	U	Fujiwara et al. (1998)	11*	Horikawa (2001)
8	Zirkuh, Iran	7.2	1997/05/10	33.40	59.96	18	D	Sudhaus and Jónsson (2011)	13	Berberian et al. (1999)
9	Manyi, Tibet	7.5	1997/11/08	35.22	87.15	20	D	Funning et al. (2007)	12	Velasco et al. (2000)
10	Fandoqa, Iran	6.6	1998/03/14	30.01	57.64	7	U	Berberian et al. (2001)	5	Berberian et al. (2001)
11	Aiquile, Bolivia	6.6	1998/05/22	−17.89	294.85	14	D	Funning et al. (2005a)	–	–
12	Izmit, Turkey	7.4	1999/08/17	40.72	30.07	20	D	Çakir et al. (2003)	12*	Li et al. (2002)
13	Hector Mine, CA., USA	7.1	1999/10/16	34.56	243.73	14	D	Simons et al. (2002)	15*	Ji et al. (2002)
14	Düzce, Turkey	7.1	1999/11/12	40.72	31.26	18	D	Burgmann et al. (2002)	22*	Umutlu et al. (2004)
15	South Seismic Zone, Iceland	6.5	2000/06/17	63.97	339.66	10	D	Pedersen et al. (2001)	–	–
16	South Seismic Zone, Iceland	6.4	2000/06/21	63.98	339.30	10	D	Pedersen et al. (2001)	–	–
17	Kokoxili, Tibet	7.8	2001/11/14	35.84	92.45	20	D	Lasserre et al. (2005)	24*	Antolik et al. (2004)
18	Nenana Mountain, AK, USA	6.7	2002/10/23	63.50	211.95	24	D	Wright et al. (2003)	–	–
19	Denali, AK, USA	7.9	2002/11/03	63.22	214.85	20	D	Wright et al. (2004b)	30*	Oglesby et al. (2004)
20	Siberian Altai, Russia	7.2	2003/09/27	49.9	87.9	15	U	Nissen et al. (2007)	18	Nissen et al. (2007)
21	Bam, Iran	6.6	2003/12/26	29.03	58.36	15	D	Funning et al. (2005b)	7	Jackson et al. (2006)
22	Al Hoceima, Morocco	6.4	2004/02/24	35.14	356.00	18	D	Biggs et al. (2006)	8	Biggs et al. (2006)
23	Parkfield, CA., USA	6.0	2004/09/28	35.8	239.6	15	D	Johanson et al. (2006)	12*	Langbein et al. (2005)
24	Chalan, Chulan, Iran	6.1	2006/03/31	33.67	48.88	9	D	Peyret et al. (2008)	6	Peyret et al. (2008)
25	South-West Iceland	6.1	2008/05/29	63.9	338.9	6	D	Decriem et al. (2010)	–	–
26	Port-au-Prince, Haiti	7.1	2010/01/12	18.5	287.4	20	D	Calais et al. (2010)	22*	Hayes et al. (2010)
27	El-Mayor Cucapah, Baja, Mexico	7.1	2010/04/04	32.2	244.7	16	D	Wei et al. (2011)	–	–
28	Yushu, China	6.8	2010/04/13	33.10	96.70	18	D	Li et al. (2011)	6	Li et al. (2011)
29	Darfield, New Zealand	7.1	2010/09/03	−43.58	172.19	14	D	Elliott et al. (2012)	7	Elliott et al. (2012)
30	Rigan, Iran	6.5	2010/12/20	28.25	59.12	13	D	Walker et al. (2013)	5	Walker et al. (2013)
31	Rigan, Iran	6.2	2011/01/27	28.15	59.04	17	D	Walker et al. (2013)	9	Walker et al. (2013)
32	Shan, Burma	6.8	2011/03/24	99.99	20.67	13	D	Feng et al. (in press)	–	–

and locking down to 20–25 km, and a relatively narrow aseismic lower crust above a Moho at 30–40 km (Fig. 5).

The 16 earthquakes with geodetic solutions in Tibet are largely in the upper 25 km of crust, with one event deeper at 31 km (Sichuan), and the interseismic locking depths, reviewed in depth in Searle et al. (2011), cover the same range (Fig. 5). However, the Moho for this region is much deeper at 50–70 km, leaving a much thicker aseismic lower crust.

Finally, the Western US has a narrower seismogenic layer of 16 km based upon the 9 earthquakes studied in this small region, and similar interseismic locking depths, estimated from extensive geodetic analyses (Fig. 5). The crust is 30–35 km thick, suggesting the aseismic lower crust is ~15–20 km thick.

Our seismogenic layer thicknesses for these regions are similar to those of Maggi et al. (2000), who used seismological constrained centroid depths. Maggi et al. (2000) also had sufficient earthquakes in Africa, the Tien Shan and North India to establish that seismogenic layer thicknesses are larger in these regions. We could not find enough geodetic studies in these regions to independently verify this result.

Table 2
Compilation of continental normal faulting earthquakes studied with InSAR. The rest of the caption is the same as in Table 1.

#	Name	M_w	Date	Lat.	Lon.	D (km)	Slip	Reference	Z (km)	Reference
1	Little Skull Mountain, CA, USA	5.6	1992/06/29	36.75	243.76	13	U	Lohman et al. (2002)	8	Romanowicz et al. (1993)
2	Nyemo, Tibet	6.1	1992/07/30	29.7	90.2	12	U	Elliott et al. (2010a, 2010b)	10	Elliott et al. (2010b)
3	Ngamring County, Tibet	6.1	1993/03/20	29.06	87.48	9	U	Funning (2005)	–	–
4	Eureka Valley, CA., USA.	6.1	1993/05/17	37.11	242.21	12	U	Massonnet and Feigl (1995)	–	–
5	Grevena, Greece	6.6	1995/05/13	40.1	21.7	15	D	Rigo et al. (2004)	11	Hatzfeld et al. (1997)
6	Aigion, Greece	6.2	1995/06/15	38.33	22.22	10	U	Bernard et al. (1997)	7	Bernard et al. (1997)
7	Dinar, Turkey	6.3	1995/10/01	38.10	30.08	13	U	Wright et al. (1999)	4	Wright et al. (1999)
8	Colfiorito, Italy	5.7	1997/09/26	43.0	12.9	7	D	Stramondo et al. (1999)	7	Hernandez et al. (2004)
9	Colfiorito, Italy	6.0	1997/09/26	43.1	12.9	7	D	Stramondo et al. (1999)	7	Hernandez et al. (2004)
10	Athens, Greece	6.0	1999/09/07	38.1	23.6	12	U	Kontoes et al. (2000)	10	Louvari and Kiratzi (2001)
11	Cankiri, Turkey	6.0	2000/06/06	40.65	33.05	8	U	Cakir and Akoglu (2008)	15*	Utkucu et al. (2003)
12	Zhongba, Tibet	6.2	2004/07/11	30.7	83.75	17	D	Elliott et al. (2010a, 2010b)	9	Elliott et al. (2010a, 2010b)
13	Zhongba, Tibet	6.2	2005/04/07	30.45	83.75	11	D	Elliott et al. (2010a, 2010b)	5	Elliott et al. (2010a, 2010b)
14	Machaze, Mozambique	7.0	2006/02/22	−21.2	33.4	25	D	Copley et al. (2012)	15	Yang and Chen (2008)
15	Gerze, Tibet	6.4	2008/01/09	32.4	85.3	12	D	Elliott et al. (2010a, 2010b)	11	Elliott et al. (2010a, 2010b)
16	Gerze, Tibet	5.9	2008/01/16	32.45	85.25	6	D	Elliott et al. (2010a, 2010b)	6	Elliott et al. (2010a, 2010b)
17	Yutian, Tibet	7.1	2008/03/20	35.4	81.5	14	D	Elliott et al. (2010a, 2010b)	7	Elliott et al. (2010a, 2010b)
18	Zhongba, Tibet	6.7	2008/08/25	30.8	83.5	19	D	Elliott et al. (2010a, 2010b)	8	Elliott et al. (2010a, 2010b)
19	Damxung, Tibet	6.3	2008/10/06	29.8	90.4	14	D	Elliott et al. (2010a, 2010b)	7	Elliott et al. (2010a, 2010b)
20	L'Aquila, Italy	6.3	2009/04/06	42.33	13.45	13	D	Walters et al. (2009)	17	Cirella et al. (2009)
21	Karonga, Malawi	6.0	2009/12/19	−10.0	34.9	6	D	Biggs et al. (2010)	5	Biggs et al. (2010)

Table 3
Compilation of continental reverse faulting earthquakes studied with InSAR. The rest of the caption is the same as in Table 1.

#	Name	M_w	Date	Lat.	Lon.	D (km)	Slip	Reference	Z (km)	Reference
1	Fawnskin, CA., USA	5.4	1992/12/04	34.35	243.09	4	U	Feigl et al. (1995)	12	Jones and Hough (1995)
2	Killari, India	6.1	1993/09/29	18.0	76.5	6	U	Satyabala (2006)	3	Seeber et al. (1996)
3	Northridge, CA., USA	6.7	1994/01/17	34.3	241.5	14	U	Massonnet et al. (1996a)	22*	Dreger (1994)
4	Sefidabeh, Iran	6.1	1994/02/23	30.9	60.5	13	D	Parsons et al. (2006)	7	Berberian et al. (2000)
5	Sefidabeh, Iran	6.2	1994/02/24	30.85	60.5	10	D	Parsons et al. (2006)	10	Berberian et al. (2000)
6	Sefidabeh, Iran	6.0	1994/02/26	30.8	60.5	13	D	Parsons et al. (2006)	5	Berberian et al. (2000)
7	Zhangbei-Shangyi, China	5.7	1998/01/10	41.14	114.44	8	D	Li et al. (2008)	–	–
8	Mt. Iwate, Japan	6.1	1998/09/03	39.80	140.90	5	D	Nishimura et al. (2001)	6*	Nakahara et al. (2002)
9	Chamoli, India	6.4	1999/03/28	30.44	79.39	13	U	Satyabala and Bilham (2006)	–	–
10	Ain Temouchent, Algeria	5.7	1999/12/22	35.2	−1.3	8	D	Belabbès et al. (2009a)	4	Yelles-Chaouche et al. (2004)
11	Bhuj, India	7.6	2001/01/26	23.51	70.27	25	D	Schmidt and Bürgmann (2006)	26*	Antolik and Dreger (2003)
12	Boumerdes-Zemmouri, Algeria	6.9	2003/05/21	36.8	3.7	20	D	Belabbès et al. (2009b)	23*	Semmane et al. (2005)
13	Miyagi, Japan	6.4	2003/07/26	38.45	141.19	6	U	Nishimura et al. (2003)	9*	Hikima and Koketsu (2004)
14	Niigata, Japan	6.8	2004/10/23	37.30	138.83	9	U	Ozawa et al. (2005)	13*	Asano and Iwata (2009)
15	Dahuiyeh (Zarand), Iran	6.4	2005/02/22	31.50	56.80	9	U	Talebian et al. (2006)	7	Talebian et al. (2006)
16	Kashmir, Pakistan	7.6	2005/10/08	34.29	73.77	14	D	Pathier et al. (2006)	17*	Avouac et al. (2006)
17	Qeshm, Iran	6.0	2005/11/27	26.88	55.89	9	U	Nissen et al. (2010)	9	Nissen et al. (2010)
18	Qeshm, Iran	6.0	2006/06/28	26.91	55.89	12	U	Nissen et al. (2010)	11	Nissen et al. (2010)
19	Noto Hanto, Japan	6.9	2007/03/25	37.22	136.66	15	U	Fukushima et al. (2008)	20*	Horikawa (2008)
20	Sichuan, China	7.9	2008/05/12	31.77	104.23	31	D	Hao et al. (2009)	35*	Nakamura et al. (2010)
21	Qeshm, Iran	6.0	2008/09/10	26.88	55.89	8	U	Nissen et al. (2010)	8	Nissen et al. (2010)
22	Qaidam, Tibet	6.3	2008/11/10	37.55	95.85	22	U	Elliott et al. (2011)	18	Elliott et al. (2011)
23	Qaidam, Tibet	6.3	2009/08/28	37.55	95.85	12	U	Elliott et al. (2011)	5	Elliott et al. (2011)
24	Christchurch, New Zealand	6.3	2011/02/21	−43.55	172.7	10	D	Elliott et al. (2012)	9*	Holden (2011)
25	Van, Turkey	7.1	2011/10/23	38.71	43.37	25	D	Elliott et al. (2013)	20	Elliott et al. (2013)

The consistency between interseismic locking depths and the depth ranges of coseismic slip release (Fig. 5), which both peak at around 10–20 km for the regions where we have sufficient data, implies that it is reasonable to estimate earthquake potential using interseismic geodetic measurements. The geodetic data therefore confirm that, for the regions where most continental earthquakes occur, the upper half of the crust is largely seismic and able to accumulate stress elastically over the earthquake cycle. Deformation occurs aseismically and continuously in the lower crust.

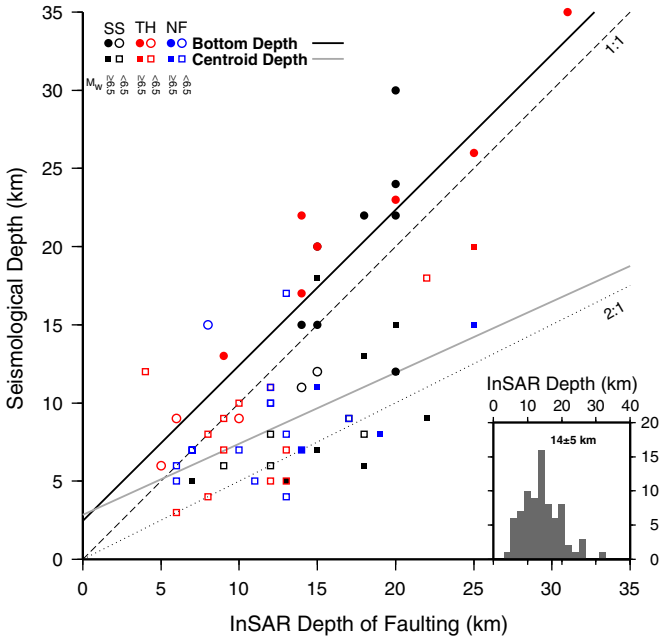

Fig. 2. Correlation between InSAR derived bottom depths of faulting given in Tables 1–3 and seismological depths from centroid estimates (squares) or bottom of distributed sources (circles). Events are coloured by mechanism: reverse (red), strike-slip (black) and normal faulting (blue). Open symbols denoted M_w < 6.5, filled Mw > 6.5. The black line is the linear regression of the InSAR depths against the seismological bottom estimates, whilst the grey line is for the seismological centroid estimates. Inset figure shows the distribution of 78 InSAR derived bottom fault depths.

5. Rheological constraints from postseismic deformation

A period of accelerated deformation is observed after many large earthquakes, in which instantaneous deformation rates are higher than those observed before the earthquake. Several mechanisms are likely occurring during this postseismic phase of the earthquake deformation cycle. Over short time scales (up to a few months), the re-equilibration of ground water levels causes a poroelastic effect (e.g. Fialko, 2004a; Jónsson et al., 2003). On longer time scales, aseismic creep on the fault plane (afterslip) and viscoelastic relaxation (VER) of the lower crust and mantle are the most significant processes.

The postseismic phase of the earthquake cycle is probably the least well observed; we found only 49 studies in the literature in which postseismic observations have been made for at least two months after the event for continental earthquakes. These studies analysed GPS and/or InSAR data from only 19 individual earthquakes and four groups of earthquakes. Furthermore, the lack of consensus on the appropriate methods for modelling postseismic deformation makes it hard to make a systematic comparison between the studies.

Most studies of postseismic deformation after large ($Mw \gtrsim 7$) earthquakes infer afterslip or viscoelastic relaxation as a deep process occurring beneath an upper layer that is modelled as a purely elastic layer. In some cases the thickness of this elastic lid is held fixed at the depth of earthquake rupture. In other studies, the elastic lid thickness is allowed to vary as a free parameter. Studies that invoke afterslip split into two camps: some carry out simple kinematic inversions to find the distribution of slip on an extended fault plane that matches the postseismic geodetic observations (e.g. Bürgmann et al., 2002); more rarely, others calculate a prediction for the amount of afterslip expected based on an assumed friction law for the fault plane (e.g. Hearn et al., 2002; Johnson et al., 2009).

Even investigations that agree that viscoelastic deformation is the dominant process occurring at depth have no consensus as to the appropriate rheology to ascribe to the viscoelastic material. Simple linear Maxwell rheologies are often used in the first instance, but these are typically unable to explain both 'early' and 'late' postseismic deformation (definitions left deliberately vague): fitting the early part of the postseismic relaxation period usually requires a lower viscosity than fitting the later part (e.g. Freed and Bürgmann, 2004; Pollitz, 2003; Ryder et al., 2007). Freed and Bürgmann (2004) showed that a non-

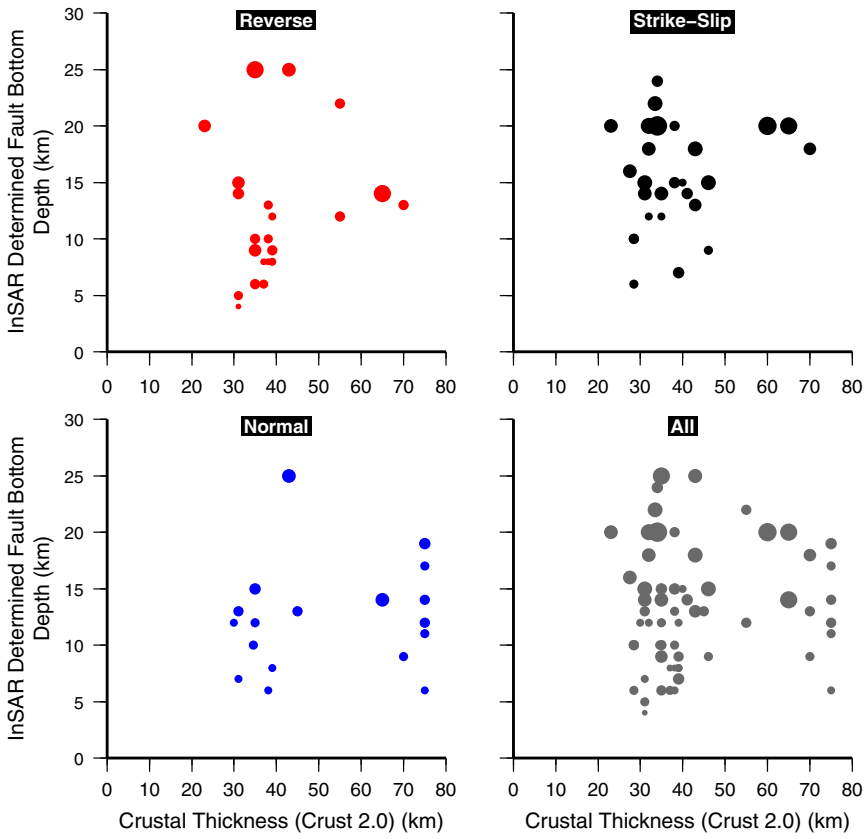

Fig. 3. Correlation between InSAR derived bottom depths of faulting given in Tables 1–3 and Crust 2.0 thickness (Bassin et al., 2000) for reverse (red), strike-slip (black), normal faulting (blue) and all events combined (grey), scaled by magnitude (M_w 5.5–7.8).

linear power-law rheology (in which strain rate is proportional to $(\text{stress})^n$) could fit both early and late postseismic deformation observed by GPS after the 1992 Landers and 1999 Hector Mine earthquakes, with $n = 3.5$. For such models to be correct, the stress change during the earthquake must dominate over the background levels of stress in the crust. Alternatively, Pollitz (2003) and others have often applied a Burgers body rheology to explain postseismic deformation. This linear rheology has two effective viscosities, which allow it to relax rapidly in the early period of postseismic relaxation and more slowly later on. Riva and Govers (2009) and Yamasaki and Houseman (2012) point out that the expected temperature structure in the lower crust and mantle can result in multiple effective viscosities for the relaxing layers — colder shallower layers relax more slowly than deeper, hot layers. Therefore, power-law or Burgers rheologies may not be required by the observations, as has previously been argued.

Yet a further complication arises because most of these models assume laterally homogeneous (layered) structures. Geological evidence suggests that shear zones develop under major crustal faults due to processes including shear heating (e.g. Thatcher and England, 1998) and grain size reduction (Bürgmann and Dresen, 2008, and references therein). Shear zones may cause lateral variations in viscosity that can also explain the geodetic observations of multiple relaxation times (Takeuchi and Fialko, 2012; Vaghri and Hearn, 2012; Yamasaki et al., 2013).

The magnitude of the earthquake being studied and the duration of observation are important factors to consider when interpreting models of postseismic deformation. Other things being equal, small earthquakes will excite less viscous flow than larger earthquakes. One might therefore expect to have to make observations over a longer time period in order to see evidence at the surface for viscoelastic relaxation at depth. By a similar line of reasoning, viscous flow will be excited in deep viscoelastic layers to a lesser extent than in shallow viscoelastic layers, and very large earthquakes may be required to excite motions in deep layers. Again, one would expect to have to observe for longer to detect a viscous flow signal. In summary, when it comes to inferring evidence for viscoelastic relaxation, the observational odds are stacked against small-magnitude earthquakes embedded in the top of a thick elastic upper layer. The optimum case for observing viscoelastic relaxation is a large earthquake occurring in a thin elastic layer.

Despite the various difficulties discussed above, we argue that there is some value in attempting to compile and compare observations of postseismic deformation globally. In Fig. 6, we summarise the results of studies that collectively model postseismic geodetic data for 19 continental earthquakes (including two earthquake sequences), plus a handful of groups of earthquakes, some of which occurred many decades ago. We are primarily interested in the depth ranges, or lithospheric layers (lower crust, upper mantle), in which different postseismic relaxation processes occur, since this gives valuable insight into the strength profile of the crust and upper mantle over the month to decadal time scale. The range of earthquake magnitudes is 5.6 to 7.9, and all case studies use data covering at least two months following the earthquake. The majority of these investigations have modelled viscoelastic relaxation (VER) and/or afterslip. The studies that only model a single process, rather than testing for both processes, are indicated in the figure by asterisks. A few studies also model poroelastic rebound.

The compilation of postseismic case studies highlights a number of key points. Firstly, even accounting for the large range of earthquake magnitudes and observation periods, there is considerable variation in inferred rheological structure between different regions around the globe (Fig. 6). Afterslip is inferred to occur anywhere from the very top of the crust right down to the upper mantle in a few cases, though some authors acknowledge that this very deep apparent afterslip may in fact be a proxy for VER. VER is inferred to occur in the lower crust in some cases (e.g. Bruhat et al., 2011; Riva et al., 2007; Ryder et al., 2007, 2011), the upper mantle in others (e.g. Biggs et al., 2009; Freed and

Table 4
Compilation of interseismic parameters studied with geodetic data.

#	Fault name[a]	Lon. (°E)	Lat. (°N)	Data source	D (km)	Reference
Tibet						
1	Altyn Tagh	79.5	36	InSAR92-99	10[b]	Wright et al. (2004a)
2	Altyn Tagh	85	37	InSAR93-00	15[b]	Elliott et al. (2008)
3	Altyn Tagh	90	38.6	GPS94-98	8–36	Bendick et al. (2000)
4	Altyn Tagh	90	38.6	GPS94-02	20	Wallace et al. (2004)
5	Altyn Tagh	90	38.6	GPS98-04	15[bc]	Zhang et al. (2007)
6	Altyn Tagh	94	39.3	GPS98-04	15[b]	Zhang et al. (2007)
7	Altyn Tagh	94	39	InSAR95-06	7–9	Jolivet et al. (2008)
8	Altyn Tagh	96	40	GPS98-04	15[b]	Zhang et al. (2007)
9	Haiyuan	104	37	InSAR93-98	0–4.2	Cavalie et al. (2008)
10	Karakoram	78.8	33.5	InSAR92-99	10[b]	Wright et al. (2004a)
11	Karakoram	78.0	34.0	InSAR92-10	15[b]	Wang and Wright (2012)
12	Lamu Co	82.5	32.5	InSAR92-99	3–5.8	Taylor and Peltzer (2006)
13	Gyaring Co	87.5	31.5	InSAR92-99	23–27	Taylor and Peltzer (2006)
14	Riganpei Co	85.75	32.5	InSAR92-99	14.5	Taylor and Peltzer (2006)
15	Kunlun	94	35	GPS98-04	15[b]	Kirby et al. (2007)
16	Kunlun	101.5	34	GPS98-04	15[b]	Kirby et al. (2007)
17	Kunlun	102.5	34	GPS98-04	15[b]	Kirby et al. (2007)
18	Manyi	87	35.2	InSAR92-97	22 ± 15	Bell et al. (2011)
19	Xianshuihe	101.2	31	GPS-07	9.2 ± 3.7	Meng et al. (2008)
20	Xianshuihe	101.8	30.3	GPS-07	1.0 ± 0.6	Meng et al. (2008)
21	Xianshuihe	100.5	31.5	GPS98-04& InSAR96-08	3–6	Wang et al. (2009a)
22	Block	84	30	GPS91-00	15[b]	Chen et al. (2004)
23	Block	88	35	GPS98-04	17[b]	Meade (2007)
24	Block	91	35	GPS & Geology	16[b]	Loveless and Meade (2011)
Himalayas						
25	MHT	81–88	27.5–30	GPS91-94	20 ± 4	Bilham et al. (1997)
26	W. MHT	79–84	28–30	GPS91-97	25.0	Larson et al. (1999)
27	W. MHT	84–92	27–28	GPS91-97	16.2	Larson et al. (1999)
28	W. MHT	76.0–80.3	29.2–33.0	GPS95-00	15	Banerjee and Bürgmann (2002)
29	W. MHT	80–84	28.2–30.0	GPS95-00	20–21	Jouanne et al. (2004)
30	W. MHT	84–90	26.5–28.2	GPS95-00	17–21	Jouanne et al. (2004)
31	W. MHT	76–83	28.5–31.5	GPS91-00	18.3	Chen et al. (2004)
32	W. MHT	83–89	27.5–28.5	GPS91-00	14.3	Chen et al. (2004)
33	W. MHT	79.5–83.5	28.0–30.0	GPS95-01	12.1	Bettinelli et al. (2006)
34	W. MHT	83.5–87.2	27.0–28.0	GPS95-01	20.4	Bettinelli et al. (2006)
35	W. MHT	79.0–89.6	27.1–28.3	GPS95-07	24.1	Banerjee et al. (2008)
36	W. MHT	78.4–84	28.5–31.5	GPS93-11	15–20	Ader et al. (2012)
37	W. MHT	84–88.1	27.5–28.5	GPS93-11	15–20	Ader et al. (2012)
38	E. MHT	89–94	27.0–27.6	GPS91-00	20.3	Chen et al. (2004)
39	E. MHT	90.0–99.8	26.9–28.5	GPS95-07	20.0	Banerjee et al. (2008)
40	Dauki	90.1–93.0	25.5–25.3	GPS95-07	37.7	Banerjee et al. (2008)
Baikal–Mongolia						
41	Bolnay	98	49.5	GPS94-02	35[b]	Calais et al. (2003)
42	Gobi Altai	98	45.5	GPS94-02	35[b]	Calais et al. (2003)
43	Tunka	101	52	GPS94-02	35[b]	Calais et al. (2003)
44	Baikal rift	107	53	GPS94-02	35[b]	Calais et al. (2003)
Iran						
45	MZP	57.2	27	GPS00-02	10–15	Bayer et al. (2006)
46	MZP	57.2	27	GPS00-08	15	Peyret et al. (2009)
47	SKJ	58	27	GPS00-02	15[b]	Bayer et al. (2006)
48	SKJ	57.7	27.7	GPS00-08	30	Peyret et al. (2009)
49	Khazar	51.5	36.7	GPS00-08	33	Djamour et al. (2010)
50	Khazar	52	36.5	GPS00-08	10	Djamour et al. (2010)
51	NTF	45	39	GPS99-09	15.5	Djamour et al. (2011)
52	NTF	47	37.5	GPS99-09	14	Djamour et al. (2011)
53	MRF	50	32	GPS97-03	10[b]	Walpersdorf et al. (2006)
54	MRF	54	29.5	GPS97-03	10[b]	Walpersdorf et al. (2006)
55	Doruneh	57	35	InSAR03-10	12[b]	Pezzo et al. (2012)
Mediterranean						
56	N. MMF	27.5	40.8	InSAR92-03	9–17	Motagh et al. (2007)
57	N. MMF	28	40.8	GPS88-97	10.5	Le Pichon et al. (2003)
58	NAF	37	40.5	GPS06-08	12.8 ± 3.9	Tatar et al. (2012)
59	NAF	38	40.25	GPS06-08	9.4 ± 3.5	Tatar et al. (2012)
60	NAF	39.2	39.9	GPS06-08	8.1 ± 3.3	Tatar et al. (2012)
61	NAF	38.8	39.9	InSAR92-99	5–33	Wright et al. (2001)
62	NAF	38.8	39.9	InSAR92-99	13.5–25	Walters et al. (2011)
63	NAF	32.5	40.8	InSAR92-02	14	Çakir et al. (2005)
64	Block	28	40.5	GPS88-97	6.5 ± 1.1	Meade et al. (2002)
65	Block	29.8	40.6	GPS88-05	18–21[b]	Reilinger et al. (2006)
66	Yammouneh	36	33–34.5	GPS02-05	13	Gomez et al. (2007)

Table 4 (*continued*)

#	Fault name[a]	Lon. (°E)	Lat. (°N)	Data source	D (km)	Reference
Mediterranean						
67	S. DSF	36	29.5–33.5	GPS96-01	12	Wdowinski et al. (2004)
68	S. DSF	36	29.5–33.5	GPS99-05	11.5 ± 10.2	Le Beon et al. (2008)
69	S. DSF (WAF)	36	29.5–31.5	GPS96-01	15 ± 5	al Tarazi et al. (2011)
70	S. DSF (JVF)	36	31.5–33.5	GPS96-01	8 ± 5	al Tarazi et al. (2011)
71	Messina	15.5	38.25	GPS94-09	7.6	Serpelloni et al. (2010)
72	S. Alps	13.2	46.5	GPS96-05	3	D'Agostino et al. (2005)
73	C. Apennines	13.5	42.5	GPS94-10	15[b]	D'Agostino et al. (2011)
74	Block	35	30	GPS96-03	13[b]	Mahmoud et al. (2005)
75	Block	36.5	35	GPS88-05	12[b]	Reilinger et al. (2006)
76	Block	355	35	GPS99-09	15[b]	Koulali et al. (2011)
77	Block	16	42	GPS	20[b]	Battaglia et al. (2004)
78	Block	26	39	GPS88-01	10[b]	Nyst and Thatcher (2004)
New Zealand						
79	C. Alpine	170	−43.5	GPS94-98	18	Moore et al. (2002)
80	C. Alpine[d]	170	−43.5	GPS94-98	22 ± 1	Beavan et al. (1999)
81	C. Alpine[d]	170	−43.5	GPS94-98	6 ± 1	Beavan et al. (1999)
82	C. Alpine	170	−43.5	GPS01-10	13–18	Beavan et al. (2010)
83	S. Alpine[d]	169	−44	GPS95-98	20 ± 2	Pearson et al. (2000)
84	S. Alpine[d]	169	−44	GPS95-98	10 ± 2	Pearson et al. (2000)
85	Awatere	173.5	−42	GPS94-04	13	Wallace et al. (2007)
86	Clarence	173	−42.3	GPS94-04	13	Wallace et al. (2007)
87	Hope	169	−42.6	GPS94-04	20	Wallace et al. (2007)
88	Wairau	173.3	−41.7	GPS94-04	20	Wallace et al. (2007)
89	Apline	170	−43.5	GPS94-04	18	Wallace et al. (2007)
Iceland						
90	RR	336	63.5	GPS93-04	9.4	Árnadóttir et al. (2009)
91	RPW	337	63.7	GPS92-00	6.6	Árnadóttir et al. (2006)
92	RPW	337	63.7	GPS00-06	4	Keiding et al. (2008)
93	RPW	337	63.7	GPS93-04	7.1	Árnadóttir et al. (2009)
94	RP	338	63.8	GPS92-00	8.3	Árnadóttir et al. (2006)
95	RP	338	63.8	GPS92-00	7	Keiding et al. (2008)
96	RP	338	63.8	GPS93-04	5.3	Árnadóttir et al. (2009)
97	SISZ	339.5	63.8	GPS92-00	19.3	Árnadóttir et al. (2006)
98	SISZ	339.5	63.8	GPS00-06	6	Keiding et al. (2008)
99	SISZ	339.5	63.8	GPS93-04	6.5	Árnadóttir et al. (2009)
100	WVZ	339.5	64.3	GPS94-03	4	LaFemina et al. (2005)
101	WVZ	339.5	64.3	GPS00-06	3	Keiding et al. (2008)
102	WVZ	339.5	64.3	GPS93-04	5.2	Árnadóttir et al. (2009)
103	EVZ	341.5	64	GPS94-03	3	LaFemina et al. (2005)
104	EVZ	341.5	64	GPS93-04	8.9	Árnadóttir et al. (2009)
105	EVZ[c]	341.5	64	GPS94-06	5/3/3	Scheiber-Enslin et al. (2011)
106	NVZ	343.5	65.5	GPS93-04	4.9	Árnadóttir et al. (2009)
107	GL	343	66.5	GPS93-04	13.8	Árnadóttir et al. (2009)
108	HFF	342.5	66.1	GPS93-04	4.7	Árnadóttir et al. (2009)
109	HFF	342.5	66.1	GPS06-10	6.3	Metzger et al. (2011)
110	KR	341.5	66.8	GPS93-04	14.5	Árnadóttir et al. (2009)
Alaska						
111	Queen Charlotte	227.5	53	GPS98-02	14[b]	Mazzotti et al. (2003)
112	Queen Charlotte	227.5	53	GPS	10[b]	Elliott et al. (2010a)
113	Malaspina Fairweather	221	60.2	GPS	5[b]	Elliott et al. (2010a)
114	Upper Fairweather	221	60.3	GPS	7.6[b]	Elliott et al. (2010a)
115	C. Fairweather	221	58.5	GPS	10[b]	Elliott et al. (2010a)
116	Glacier Bay	224	59	GPS	10[b]	Elliott et al. (2010a)
117	Boundary	223	59.7	GPS	8[b]	Elliott et al. (2010a)
118	Foothills	222	58.8	GPS	4.98–12[b]	Elliott et al. (2010a)
119	Fairweather	221	59.7	GPS92-02	9.0 ± 0.8	Fletcher and Freymueller (2003)
120	Transition	220	58.5	GPS	8/26.5[b]	Elliott et al. (2010a)
121	Denali	221.5	61	GPS92-02	10[b]	Fletcher and Freymueller (2003)
122	Denali	221.5	61	GPS	10[b]	Elliott et al. (2010a)
123	Denali	214	63.5	InSAR92-02	10[b]	Biggs et al. (2007)
Western United States						
124	Wasatch	248	40	GPS96-08	7 ± 3	Soledad Velasco et al. (2010)
125	Imperial	244.5	32.8	GPS99-00	10	Lyons et al. (2002)
126	Imperial	244.5	32.7	GPS	5.9 ± 3	Smith-Konter et al. (2011)
127	SAF	244.2	33.5	InSAR92-00	17	Fialko (2006)
128	SM	244.2	32.8	GPS	10.8 ± 1.1	Smith-Konter et al. (2011)
129	ETR	244	34.0	GPS94-09	15[b]	Spinler et al. (2010)
130	Borrego	244	33.2	GPS	6.4 ± 1.4	Smith-Konter et al. (2011)
131	DV-FC	244	35.5	GPS94-99	15[b]	Gan et al. (2000)
132	DV	244	35.5	GPS99-03	12[b]	Wernicke et al. (2004)
133	DV-FC	244	35.5	GPS	7.5 ± 2.7	Hill and Blewitt (2006)

(*continued on next page*)

Table 4 (*continued*)

#	Fault name[a]	Lon. (°E)	Lat. (°N)	Data source	D (km)	Reference
Western United States						
134	Coachella	244	33.7	GPS	11.5 ± 0.5	Smith-Konter et al. (2011)
135	SJF	244	33.2	InSAR92-00	12	Fialko (2006)
136	Coyote Creek	243.7	33.2	GPS	6.3 ± 2	Smith-Konter et al. (2011)
137	Anza	243.5	33.5	GPS	13.7 ± 3.2	Smith-Konter et al. (2011)
138	YM	243.5	36.8	GPS	12.8 ± 2.3	Hill and Blewitt (2006)
139	SP	243.5	36.7	GPS99-03	12[b]	Wernicke et al. (2004)
140	Palm Springs	243.5	34	GPS	16.4 ± 8	Smith-Konter et al. (2011)
141	SB	243	34	GPS	17.8 ± 2	Smith-Konter et al. (2011)
142	PV-HM	243	36	GPS94-99	15[b]	Gan et al. (2000)
143	PV-HM	243	36	GPS	8.6 ± 3.7	Hill and Blewitt (2006)
144	SJV	243	34.8	GPS	21.5 ± 6.3	Smith-Konter et al. (2011)
145	SJM	242.5	34	GPS	21.0 ± 3.2	Smith-Konter et al. (2011)
146	LL-BW	242.5	35.5	InSAR92-00	5	Peltzer et al. (2001)
147	HM	242.2	36.6	InSAR92-00	2 ± 0.4	Gourmelen et al. (2010)
148	OV	242	36	GPS	7.3 ± 4.0	Hill and Blewitt (2006)
149	OV	242	36	GPS94-99	15[b]	Gan et al. (2000)
150	Mojave	242	34.5	GPS	15[b]	Johnson et al. (2007)
151	Mojave	242	34.5	GPS	18–24	Johnson et al. (2007)
152	Mojave	242	34.5	GPS	16.8 ± 0.4	Smith-Konter et al. (2011)
153	Carrizo	240.5	35	GPS	18.7 ± 2	Smith-Konter et al. (2011)
154	SA	240	35	GPS	10.2 ± 3.8	Hill and Blewitt (2006)
155	GVF	237.7	38.4	GPS/InSAR	5	Jolivet et al. (2009)
156	RCF	237.5	38.2	GPS/InSAR	10	Jolivet et al. (2009)
157	SAF	237.2	38	GPS/InSAR	10 ± 2	Jolivet et al. (2009)
158	Block	242	39	GPS	15[b]	Hammond et al. (2011)
159	Block	241	40	GPS	15[b]	Hammond and Thatcher (2007)
Sumatran						
160	Sumatran	100	0	GPS89-93	15	Prawirodirdjo et al. (1997)
161	Sumatran	100.7	−0.8	GPS89-96	22 ± 12	Genrich et al. (2000)
162	Sumatran	100.4	−0.4	GPS89-96	24 ± 13	Genrich et al. (2000)
163	Sumatran	100	0.6	GPS89-96	56 ± 35	Genrich et al. (2000)
164	Sumatran	99.4	1.3	GPS89-96	21 ± 12	Genrich et al. (2000)
165	Sumatran	98.8	2.2	GPS89-96	9 ± 3	Genrich et al. (2000)
166	Sumatran	98.4	2.7	GPS89-96	9 ± 4	Genrich et al. (2000)
Southeast Asia						
167	Sagaing	96	22	GPS98-00	15	Socquet et al. (2006b); Vigny et al. (2003)
168	Sagaing	96	26	GPS05-08	7.7	Maurin et al. (2010)
169	Sagaing	96	24	GPS05-08	6.3	Maurin et al. (2010)
170	Sagaing	96	22	GPS05-08	20.3	Maurin et al. (2010)
171	Palu-Koro	120	−1	GPS92-05	12	Socquet et al. (2006a)
172	Gorontalo	122.5	1	GPS92-05	10	Socquet et al. (2006a)
173	Lawanopo	122	−3	GPS92-05	15	Socquet et al. (2006a)
174	Tomini	122	−0.3	GPS92-05	15	Socquet et al. (2006a)
Central America						
175	El Pilar	296.5	10.5	GPS94-00	14 ± 2	Pérez et al. (2001)
176	Septentrional	288	20	GPS86-95	15	Dixon et al. (1998)
177	Septentrional	288	20	GPS94-01	15[b]	Calais et al. (2002)
178	Enriquillo	287	18.5	GPS86-95	15	Dixon et al. 1998
179	Enriquillo	287	18.5	GPS94-01	15[b]	Calais et al. (2002)
180	NH	288	20.4	GPS86-95	15	Dixon et al. (1998)
181	NH	288	20.4	GPS94-01	15[b]	Calais et al. (2002)
182	PMFS	270.5	15	GPS99-03	21	Lyon-Caen et al. (2006)
183	PMFS	270.5	15	GPS99-06	20	Franco et al. (2012)
184	Block	282.5	18.3	GPS98-11	15[b]	Benford et al. (2012)
Taiwan						
185	Tainan	120.19	23	GPS/InSAR	4[b]	Huang et al. (2009)
186	Houchiali	120.24	23	GPS/InSAR	4[b]	Huang et al. (2009)
187	Chungchou	120.26	23	GPS/InSAR	4.1[b]	Huang et al. (2009)

[a] Block: block model with constant locking depth; CJFS: Central Jamaica Fault System; DSF: Dead Sea Fault; DV-FC: Death Valley-Furnace Creek; ETR: Eastern Transverse Ranges Province; EVZ: Eastern Volcanic Zone; GL: Grimsey Lineament; HFF: Husavik-Flatey Fault; JVF: Jordan Valley Fault; KR: Kolbeinsey Ridge; LL-BW: Little Lake-Black Water Fault; MHT: Main Himalayan Thrust; MRF: Main Recent Fault; MZP: Zendan–Minab–Palami Fault; NAF: North Anatolian Fault; NH: North Hispaniola; N. MMF: Northern Marmara Fault; NTF: North Tabriz Fault; NVZ: Northern Volcanic Zone; OV: Owens Valley; PMFS: Polochic–Motagua Fault System; PV-HM: Panamint Valley-Hunter Mountain; RP: Reykjanes Peninsula; RPW: Western Reykjanes Peninsula; RR: Reykjanes Ridge; SA: San Andreas; SB: San Bernardino; SISZ: South Iceland Seismic Zone; SJF: San Jacinto Fault; SJM: San Jacinto Mountain; SJV: San Jacinto Valley; SKJ: Sabzevaran-Kahnuj-Jirsoft Fault; SM: Superstition Mountain; SP: Satellite-Pahrump; WAF: Wadi Araba Fault; WVZ: Western Volcanic Zone; YM: Yucca Mountain; YZS: Yarlung-Zangbo Suture.

[b] Fixed locking depth.

[c] Corresponding to three profiles in the literature.

[d] For single and two fault models respectively.

Bürgmann, 2004; Johnson et al., 2009; Pollitz et al., 2012), and sometimes in both (e.g. Hearn et al., 2009; Vergnolle et al., 2003; Wang et al., 2009b). We note, however, that even if the spatial pattern of the data clearly indicates viscoelastic relaxation, actual viscosity values for a particular layer are commonly poorly-resolved by the data, which leads to some uncertainty in how VER varies with depth. This issue of resolution for postseismic data has been explored in detail by Pollitz and Thatcher (2010). In Fig. 6, the dashed yellow lines indicate depth ranges where (a) viscosities are poorly-constrained, and/or (b) viscosities are several times higher than in the other layer. Both cases go under the label of "possible VER", as opposed to "dominant VER" (solid yellow lines).

Since different studies use different data sets with different resolving capabilities, it is important to consider the interpretations for a particular earthquake or region in aggregate. In some regions there is a clear signature of viscoelastic relaxation in the upper mantle. In the Basin and Range province, mantle VER has been clearly inferred in five separate studies of individual earthquakes (Hector Mine 1997 (Pollitz, 2003); Hebgen Lake 1959 (Reilinger 1986, Nishimura & Thatcher, 2003); and Landers 1992 (Pollitz et al., 2000, Fialko 2004a), as well as for groups of historic earthquakes that occurred in the Central Nevada Seismic Belt. The four Basin and Range studies that infer only afterslip/poroelastic mechanisms (no VER) did not attempt to model VER (Massonnet et al., 1996b; Peltzer et al., 1998; Perfettini and Avouac, 2007; Savage and Svarc, 1997). A fifth study (Fialko, 2004a) does not model VER explicitly, but as a comment on far-field residuals resulting from afterslip-only modelling, mentions that mantle VER may also have occurred. Only one paper concludes VER in the lower crust (Deng et al., 1998), but Pollitz et al. (2000) and Pollitz (2003) suggest that VER may have occurred in the lower crust as well as the upper mantle, with viscosities at least a factor of two higher in the lower crust. The other earthquake that seems to offer clear evidence for upper mantle VER is the 2002 Denali earthquake in Alaska. The four studies of this event all infer VER in the mantle, with no flow in the lower crust (e.g. Biggs et al., 2009; Freed et al., 2006; Johnson et al., 2009; Pollitz, 2005). Of those, the three studies that also model afterslip conclude that afterslip in the lower crust accompanied mantle VER. For the 1999 Izmit earthquake on the North Anatolian Fault, short time-scale (a few months) observations lead to conclusions of afterslip only (Bürgmann et al., 2002; Hearn et al., 2002; Reilinger et al., 2000), but longer time-scale (a few years) observations lead to inferences of VER in the lower crust and upper mantle (Hearn et al., 2009; Wang et al., 2009b). For two M_w 6.5 earthquakes in Iceland in 2002, Jónsson (2008) infers from four years of geodetic data that VER took place in the upper mantle, although initial data only revealed poroelastic rebound (Jónsson et al., 2003).

In some regions there is strong evidence for viscoelastic relaxation having occurred primarily in the lower crust, rather than the upper mantle. Along the San Andreas Fault system, multi-year observations following the 2004 Parkfield, 1994 Northridge and 1989 Loma Prieta earthquakes indicate lower crustal VER. Again, there are also studies which only solve for afterslip. The study by Freed (2007), on the other hand, investigated both processes, but concluded that only afterslip occurred during the first two years after the Parkfield earthquake. A later study of the same event by Bruhat et al. (2011) used six years of postseismic data and suggested that VER in the lower crust accompanied afterslip in the upper crust, although the authors acknowledge that observations of localised tremor in the lower crust (Shelly and Johnson, 2011) support the occurrence of deep afterslip. Lower crustal VER has also been inferred in studies of earthquakes in Italy, Taiwan and Tibet. In general, smaller earthquakes do not appear to excite flow in the upper mantle, but larger earthquakes at the same locations may be able to. One earthquake in Tibet where VER has not been inferred at any depth was the 2008 Nima-Gaize event (Ryder et al., 2010). This was a small (M_w 6.4) earthquake and the InSAR data used only covered the first nine postseismic months. Viscoelastic relaxation was not ruled out by these short time-scale data; rather, the lack of VER signature was used to place a lower bound on possible viscosities in the lower crust.

Because of the wide variety of approaches used in modelling viscoelastic relaxation, we do not include viscosity values in our compilation in Fig. 6. A detailed comparison of modelling efforts is beyond the scope of this paper. Nevertheless, it is helpful to consider the range of viscosities inferred in postseismic studies, and identify some general patterns. For the viscoelastic layers (lower crust or upper mantle) where viscosity is well-constrained, the range of Maxwell viscosities across all studies is 1×10^{17}–7×10^{19} Pa s. Where other linear viscoelastic rheologies are used (standard linear solid, Burgers), the range is 1×10^{17}–2×10^{20} Pa s. It should be noted that for poorly-constrained layers, several studies estimate a lower bound. For example, Gourmelen and Amelung (2005) can only constrain the viscosity of the lower crust in the CNSB to be $>1 \times 10^{20}$ Pa s. The overall viscosity range for the well-constrained layers gives a range of relaxation times from one month up to 200 years. For the poorly-constrained layers, relaxation times may be longer than 200 years. Many short time scale (<10 year) studies have concluded that apparent viscosity increases with time following an earthquake. However, the modern studies of ongoing relaxation around earthquakes that occurred several decades ago do not consistently find higher viscosities than shorter postseismic studies of more recent earthquakes.

To summarise the results from the entire postseismic compilation: of the ~20 individual earthquakes/sequences considered, 16 have VER inferred by at least one study. Of the four that do not, two (L'Aquila and Nima-Gaize) are small magnitude (M_w 6.3 and 6.4 respectively) and only have a short period of observation (6 and 9 months respectively), and so would not be expected to have excited observable deep viscous flow. The other two are the Zemmouri and Mozambique earthquakes in Africa. These are larger magnitude (M_w 6.9 and 7) events and have been observed for longer (at least 2.5 years). A broad-brush conclusion is that viscoelastic relaxation in the lower crust and/or upper mantle is to be expected after most large earthquakes (but may only be detected with very long periods of observations). This in turn implies that there is not much long-term strength beneath the elastic upper crust, at least in fault zones.

6. Discussion

6.1. Influence of the Moho depth and geothermal gradient on the earthquake cycle

Our initial aim in this paper, in line with the theme of this special volume, was to test whether crustal thickness had any appreciable influence on the deformation observed during the earthquake cycle. The most robust parameter that we have been able to extract is the thickness of the seismogenic layer, which we find to be consistent between coseismic and interseismic investigations. We find, in line with previous seismic studies (e.g. Jackson et al., 2008; Maggi et al., 2000), that there is no simple global relationship between seismogenic layer thickness and crustal thickness. In fact, seismogenic layer thickness is remarkably constant in the regions where we have sufficient data for robust analysis, whereas crustal thicknesses in the same regions vary by a factor of two or more.

Ultimately, the seismogenic layer thickness is limited by the depth at which creep processes allow tectonic stresses to be relieved aseismically and this, in turn, is a function of lithology, grain-size, water content, strain rate and temperature. In the oceanic lithosphere, where lithology is fairly constant, temperature is the dominant factor, with earthquakes only occurring in the mantle at temperatures below ~600 °C (e.g. McKenzie et al., 2005). We test whether temperature exerts a dominant control globally on seismogenic layer thickness in continental lithosphere by using direct and indirect measures of crustal heat flow.

Firstly, we use a global compilation of direct heat flow measurements by Hasterok and Chapman (2008), updated from Pollack et al. (1993). The heat flow data set is noisy and highly uneven in its distribution, with high sample densities in regions such as Europe and North America and lower

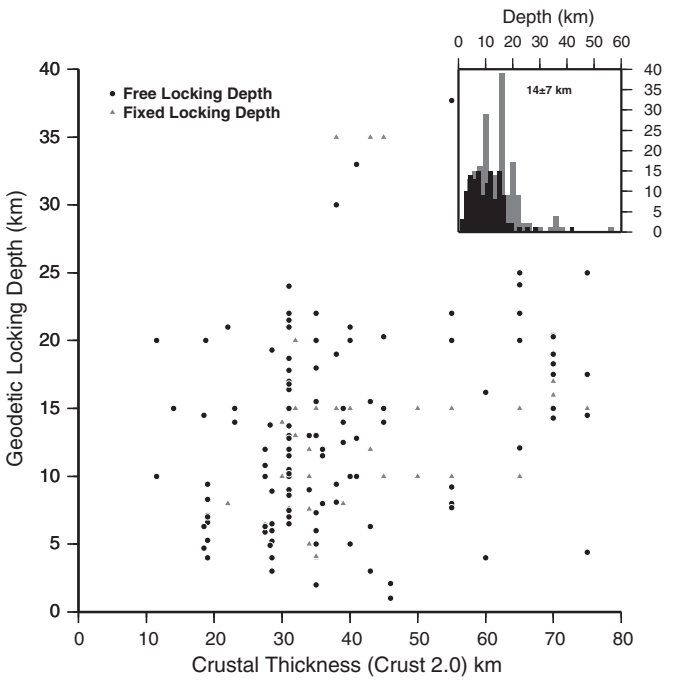

Fig. 4. Correlation between interseismic locking depth (Table 4) and Crust 2.0 thickness (Bassin et al., 2000). Symbols indicate whether the locking depth was fixed (triangles) or free to vary (circles) in the respective study. Inset figure shows the distribution of 187 geodetically derived locking depths separated by free (black) and fixed (grey).

sampling in Asia. To provide a continuous grid against which to compare average heat flows with the earthquake depths, we first take median samples of the data at 0.5 degree spacing. We then interpolate (Smith and Wessel, 1990) to 1 degree spacing to cover regions in which no direct heat flow data are available. We do not recover an inverse relationship between the deepest extent of faulting and average heat flow (Fig. 7).

Secondly, we use lithospheric thickness, derived from surface wave tomography (Priestley and McKenzie, 2006), as a proxy for geothermal gradient; areas with thick lithosphere should have relatively low geothermal gradient and hence have a relatively thick seismogenic layer. We also see no clear relationship between lithospheric thicknesses and our estimates of seismogenic thickness (Fig. 7).

On a local scale, there is a clear relationship between the geothermal gradient and the seismogenic layer thickness. This is clearly shown by microseismicity studies in regions such as California (e.g. Nazareth and Hauksson, 2004; Sibson, 1982), and Iceland (e.g. Ágústsson and Flóvenz, 2005; Björnsson, 2008). But there is no obvious global relationship between thermal structure and seismogenic layer thickness evident in our compilations. The effect of temperature, which is clear in oceanic lithosphere and in small regions, is masked in the continents by spatial variations in lithology, strain-rate, and grain size.

6.2. Seismogenic and elastic thicknesses — implications for the rheology of continental lithosphere

Starkly different estimates for elastic thickness (T_e) have been at the core of the debate about the rheology of continental lithosphere (e.g. Burov and Watts, 2006; Jackson et al., 2008). Several different methods have been used to derive T_e. One method, probably the most commonly applied, relies on the spectral coherence between the Bouguer gravity anomaly and topography (Forsyth, 1985). Audet and Bürgmann (2011) recently used this method to produce a global map of elastic thickness, giving values that are typically much larger than the seismogenic thicknesses estimated in this paper and elsewhere (Fig. 5). For example, in Iran, Audet and Bürgmann (2011) estimate T_e at 35–65 km, but no earthquake occurs deeper than ~20 km. McKenzie and Fairhead (1997) showed that estimates of T_e obtained from Bouguer gravity anomalies are upper bounds, since short-wavelength topography has been removed or modified by surface processes. Instead, they advocate using either the admittance between topography and free-air gravity or direct flexural models of free-air gravity profiles. These typically yield much lower values for T_e, which are always less than the seismogenic thickness (Fig. 5; Jackson et al., 2008; McKenzie and Fairhead, 1997; Maggi et al., 2000; Sloan et al., 2011). However, Pérez-Gussinyé et al. (2004) suggest that the McKenzie and Fairhead (1997) estimates of T_e may, in turn, be biased towards lower values due to differences in windowing between theoretical and observed admittances.

No global grid exists for T_e from free-air methods, so we compared the Audet and Bürgmann (2011) global grid with our geodetic estimates of seismogenic thickness, T_s (Fig. 7), and find that these estimates of T_e are almost always significantly greater than T_s. Furthermore, we find no correlation between T_s and T_e derived in this way. By contrast, regional estimates of T_e derived from free-air gravity (Fig. 5) are consistently less than geodetic estimates of T_s, as is the case for seismic estimates of T_s. For the regions where there are sufficient geodetic data to estimate T_s, we found it to be fairly constant. Likewise, there is little variation in free-air T_e in these areas. Maggi et al. (2000) found that in regions where deeper earthquakes do occur in the lower crust (Africa, the Tien Shan and North India), T_e estimated from free-air methods is higher, although it is always significantly lower than estimates derived from Bouguer coherence.

We do not wish to use this manuscript to question the validity of either method for estimating elastic thickness for the crust, as extensive literature on this already exists (e.g. Crosby, 2007; McKenzie and Fairhead, 1997; Pérez-Gussinyé et al., 2004). Having said that, the widespread inferences of aseismic deformation in the lower crust and upper mantle, required to explain geodetic observations of postseismic motions, are hard to reconcile conceptually with these regions supporting significant topographic loads over geologic timescales: postseismic relaxation times are on the order of a few months to a few hundred years. Geodetic observations of the seismic cycle therefore appear to support the lower estimates of T_e, and hence the concept that the strength of continental lithosphere is concentrated in the upper seismogenic layer (the "crème brûlée" model).

Of course, sampling continental rheology through observations of the earthquake loading cycle is an inherently biased process. Earthquakes are not uniformly distributed throughout the continental lithosphere, and preferentially sample areas with lower T_e estimated with either Bouguer or Free-air gravity methods (e.g. Fig. 1), presumably because earthquakes are occurring in the weakest regions (e.g. Tesauro et al., 2012). In addition, fault zones are capable of modifying their local rheology through processes such as shear heating and grain size reduction, which act to create local weak shear zones at depth (Bürgmann and Dresen, 2008). Observations of postseismic relaxation could therefore be sampling weak regions within an otherwise strong crust or mantle (the "banana split" model of Bürgmann and Dresen (2008)). This is consistent with studies of glacial isostatic adjustment, which often suggest thick elastic lids (e.g. Watts et al., 2013). If only fault zones are weak, topographic loads could still be supported over geologic timescales by stronger regions away from them and higher estimates of T_e could be valid. Such a view would be consistent with the idea that the continents behave as a series of independent crustal blocks (e.g. Meade, 2007; Thatcher, 2007). Dense geodetic observations of deformation in regions including Greece, Tibet and the Basin and Range, however, suggest that such blocks are small, if they exist, with dimensions comparable to the thickness of the crust (e.g. Floyd et al., 2010; Hammond et al., 2011; Wang and Wright, 2012).

7. Conclusions

We have compiled geodetic estimates of seismogenic layer thickness from the coseismic and interseismic phases of the earthquake loading

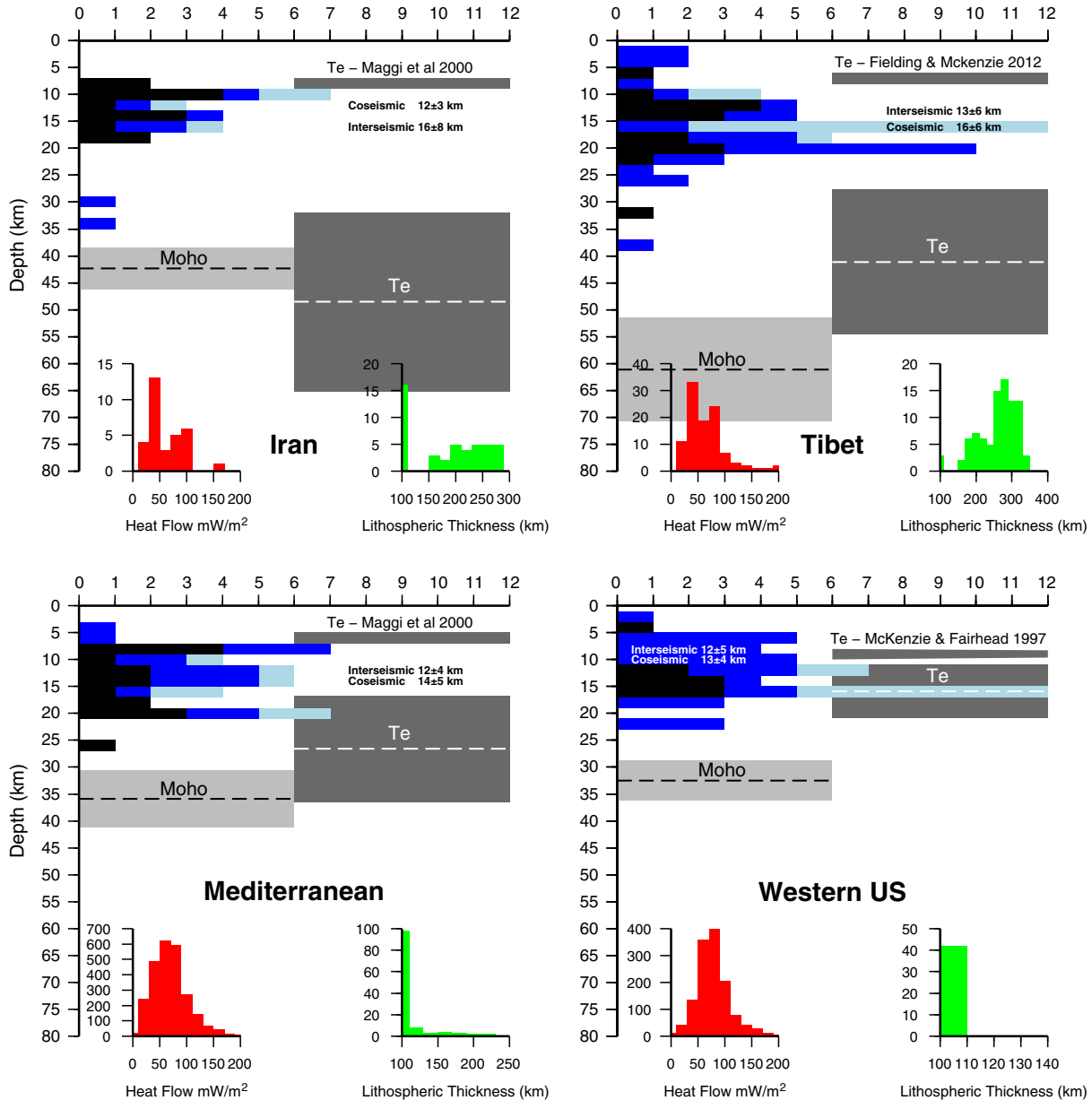

Fig. 5. Histograms of earthquake rupture bottom depths (black bars) determined from InSAR-constrained coseismic slip models based upon the data in Tables 1–3, grouped by four continental regions shown in Fig. 1. Blue bars are from the locking depths of interseismic studies shown in Table 4, for fixed (light-blue) and estimated depths (dark-blue). The mean (dashed line) Moho depths (Fig. 1b) and one standard deviation (light grey panel) within each region are from the Crust 2.0 model (Bassin et al., 2000). The mean (dashed white line) elastic thicknesses (T_e) from Audet and Bürgmann (2011) and one standard deviation (dark grey panel) within each region are also shown. Elastic thicknesses from individual studies using free-air gravity are also shown from Fielding and McKenzie (2012), Maggi et al. (2000), and McKenzie and Fairhead (1997). The inset red histograms show the distribution of heat flow within the region from the database updated by Hasterok and Chapman (2008). The inset green histograms show the distribution of lithospheric thickness within the region from Priestley and McKenzie (2006). Note the method used by Priestley and McKenzie (2006) cannot resolve lithospheric thicknesses less than 100 km.

cycle, and find no significant relationship with the depth of the Moho. For the regions where there are sufficient geodetic data to obtain robust results, the seismogenic layer thickness determined from both coseismic geodetic slip inversions and interseismic locking depth analyses is reasonably constant between regions, despite considerable variation in crustal thickness.

We find rupture depths inferred from coseismic geodetic slip inversions to be consistent with depths from seismology bodywave inversions. In the regions where there are sufficient data, the interseismic "locking depth" estimates are also consistent with the seismogenic layer thickness found coseismically. This implies that interseismic geodetic observations are reliable indicators of earthquake potential.

The transition from frictional controlled faulting to aseismic creeping processes usually occurs in the mid crust and is thought to be dependent on lithology, strain-rate, grain-size, water content and temperature. We found no relationship between the seismogenic thickness and geothermal gradient (measured directly or inferred from lithospheric thickness models). This suggests that the effect of temperature, which is so clear in oceanic lithosphere, is masked in the continents by considerable variation in lithology, strain-rate and grain size.

Elastic thicknesses derived from the coherence between Bouguer gravity and topography is systematically larger than the seismogenic thickness estimated geodetically, but there is no obvious correlation between them. By contrast, as has previously been shown, elastic thicknesses from free-air gravity methods are typically smaller than seismogenic layer thicknesses; although there are no geodetic results in regions where Maggi et al. (2000) found high T_e and high T_s, the

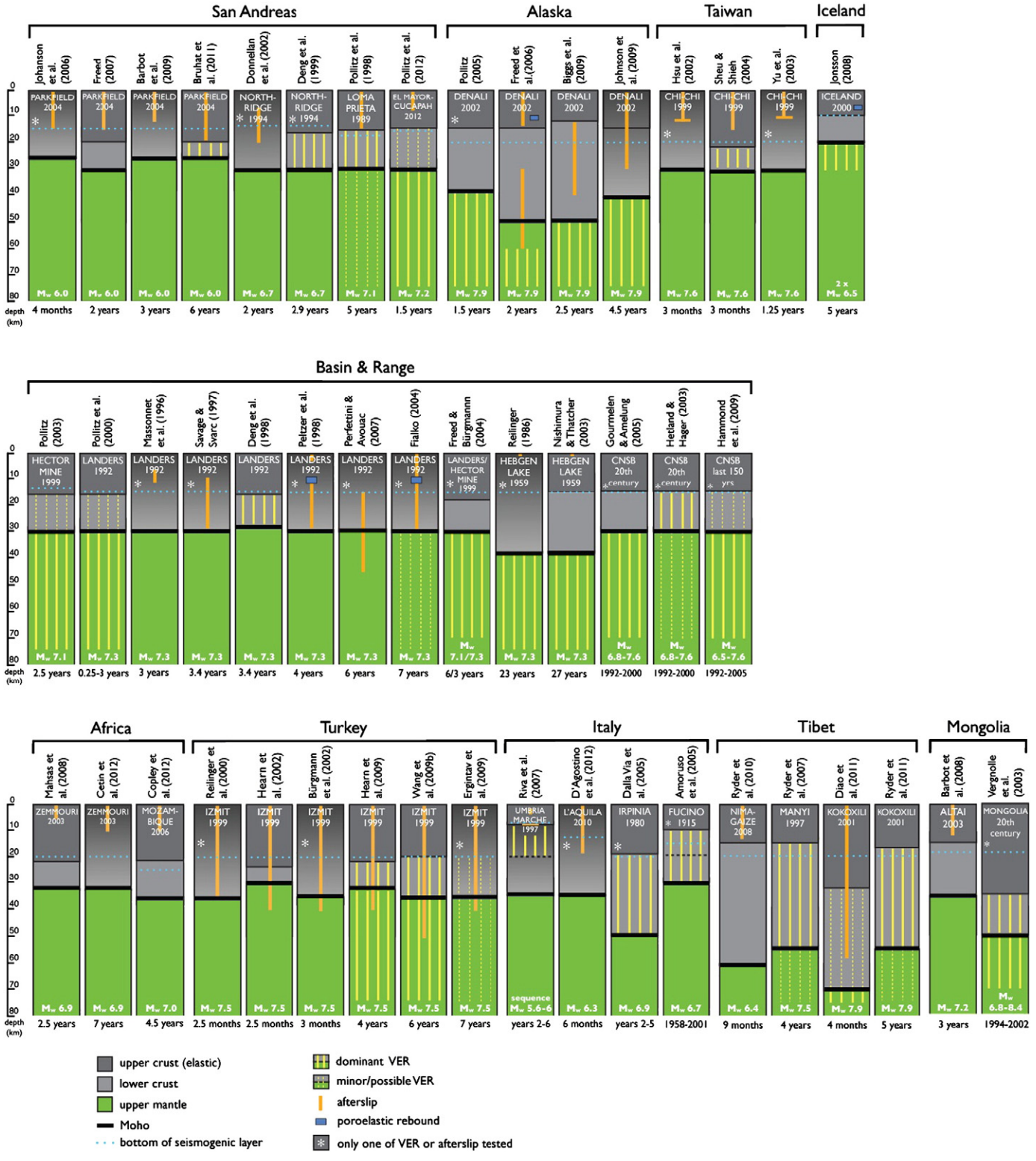

Fig. 6. Global compilation of rheological interpretations of postseismic geodetic data. VER = viscoelastic relaxation. Each column represents a single case study, either for an individual earthquake or a group of earthquakes. Grey background denotes crust and green background denotes mantle. Where the crust is divided into upper and lower layers, upper crustal thickness is either assumed to be the maximum rupture depth/seismogenic thickness for the area, or is directly estimated from the geodetic data. The magnitude of each earthquake is given at the bottom of each column (white text), along with the geodetic observation period (black text). A white asterisk means that the study only investigated a single relaxation process (either afterslip or viscoelastic relaxation). Minor/possible VER implies that viscosities for a particular layer are poorly-constrained, and/or are within one order of magnitude greater than for the layer where dominant VER occurs. Seismogenic thickness is marked for reference (light blue dotted lines). The figure summarises the results of the following studies: Amoruso et al., 2005; Barbot et al., 2008; Barbot et al., 2009; Biggs et al., 2009; Bruhat et al., 2011; Cetin et al., 2012; Copley et al., 2012; D'Agostino et al., 2012; Dalla Via et al., 2005; Deng et al., 1998; Deng et al., 1999; Diao et al., 2011; Donnellan et al., 2002; Ergintav et al., 2009; Fialko, 2004; Freed, 2007; Freed and Burgmann, 2004; Freed et al., 2006; Gourmelen and Amelung, 2005; Hammond et al., 2009; Hearn et al., 2002; Hetland and Hager, 2003; Hsu et al., 2002; Johanson et al., 2006; Jónsson, 2008; Johnson et al., 2009; Mahsas et al., 2008; Massonnet et al., 1996; Nishimura and Thatcher, 2003; Peltzer et al., 1998; Perfettini and Avouac, 2007; Pollitz, 2003; Pollitz, 2005; Pollitz et al., 2000; Pollitz et al., 1998; Pollitz et al., 2012; Reilinger, 1986; Reilinger, 2006; Reilinger et al., 2000; Riva et al., 2007; Ryder et al., 2007; Ryder et al, 2010; Ryder et al., 2011; Savage and Svarc, 1997; Sheu and Shieh, 2004; Vergnolle et al., 2003; Wang et al., 2009b; Yu et al., 2003.

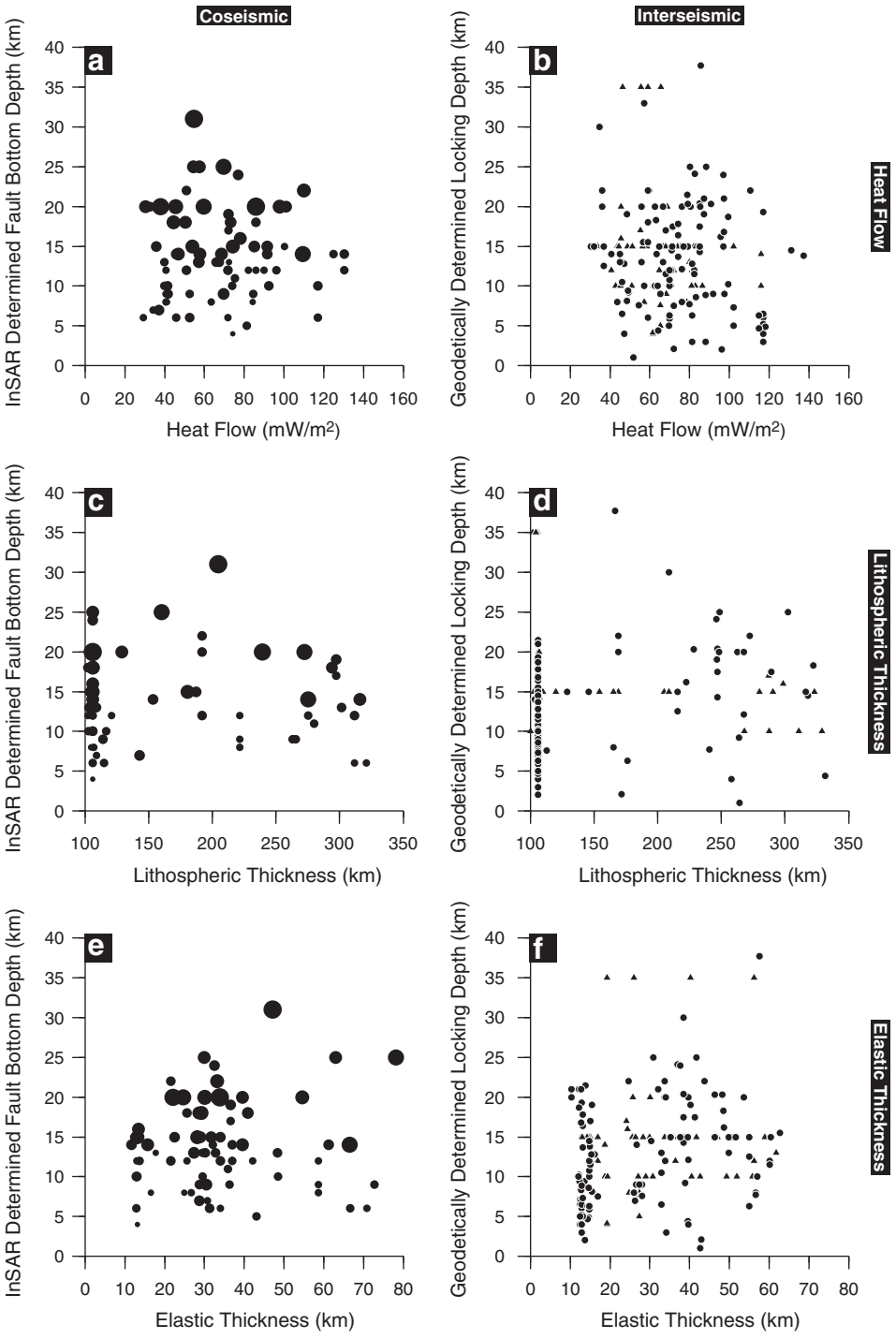

Fig. 7. Correlation between InSAR-derived bottom depths of faulting given in Tables 1–3, or geodetically-determined locking depths given in Table 4, and elastic thickness (T_e) (Audet and Bürgmann, 2011), lithospheric thickness (Priestley and McKenzie, 2006) and heat flow (Hasterok and Chapman, 2008). The method used by (Priestley and McKenzie, 2006) cannot resolve lithospheric thicknesses less than 100 km. Coseismic events are scaled by magnitude (M_w 5.5–7.8); interseismic locking depths are plotted as circles if they were determined by free inversion, or triangles if they were held fixed.

consistency of seismogenic thicknesses from geodesy and seismology suggests that this relationship will hold.

The rapid relaxation of the lower crust and/or upper mantle observed in many places is hard to reconcile with the higher estimates of T_e — relaxation times are typically observed to be a few months to a few centuries. Our analysis of the geodetic data therefore supports the "crème brûlée" model, in which the strength of the continental lithosphere is supported in the upper seismogenic layer.

However, we note that geodetic observations of the earthquake cycle are inherently biased in their distribution. Furthermore, fault zones modify the rheology of the crust and mantle in which they sit through processes including grain-size reduction and shear heating. The weak material that responds in the postseismic period may therefore not be representative of the bulk rheology of the continental lithosphere: Postseismic results could be sampling weak regions within an otherwise strong crust or mantle (the "banana split" model of Bürgmann and Dresen (2008)). Studies of glacial or lake loading/unloading may not suffer from this bias.

Our compilation suffers from the relatively short time that satellite geodetic methods have been available, a lack of truly global coverage

(in comparison to seismology), and from the variations in modelling strategies applied by different groups. Specifically, we lack sufficient geodetic observations from areas where Maggi et al. (2000) and others have inferred thicker seismogenic layers. In addition, postseismic deformation results are too scarce, and modelling strategies too variable, to form a robust global picture. With the start of the 20-year Sentinel-1 SAR satellite programme in 2013, systematic, dense geodetic observations will be made globally for the first time, dramatically increasing the availability and reliability of geodetic observations of the earthquake loading cycle. We strongly recommend that the geodetic community follows the lead of the seismological community by measuring, modelling and cataloguing coseismic, interseismic and postseismic deformation in a routine, systematic fashion.

Acknowledgements

This work was supported in part by the Natural Environmental Research Council (NERC) through the National Centre of Earth Observation (NCEO) of which the Centre for the Observation and Modelling of Earthquakes, Volcanoes & Tectonics (COMET, http://comet.nerc.ac.uk) is a part. Crust 2.0 (Bassin et al., 2000) was downloaded from http://igppweb.ucsd.edu/gabi/rem.html. We are grateful to Pascal Audet and Roland Bürgmann for making their global Elastic Thickness data set available, and to Dan McKenzie and Keith Priestley for sharing their lithospheric thickness data. Global heat flow data were taken from the Global Heat Flow Database of the International Heat Flow Commission (www.heatflow.und.edu). This manuscript was improved by constructive reviews from Roland Bürgmann and an anonymous reviewer, and we are grateful for additional comments from Tony Watts, Alex Copley and Al Sloan. Most figures were made using the public domain Generic Mapping Tools (Wessel and Smith, 1998). TJW was funded by the Royal Society through a University Research Fellowship. HW is supported by the NSFC (41104016).

References

Ader, T., Avouac, J.P., Liu-Zeng, J., et al., 2012. Convergence rate across the Nepal Himalaya and interseismic coupling on the main Himalayan thrust: implications for seismic hazard. Journal of Geophysical Research 117, B04403. http://dx.doi.org/10.1029/2011JB009071.

Ágústsson, K., Flóvenz, Ó.G., 2005. The thickness of the seismogenic crust in Iceland and its implications for geothermal systems. Proceedings of the World Geothermal Congress, pp. 24–29.

al Tarazi, E., Abu Rajab, J., Gomez, F., 2011. GPS measurements of nearfield deformation along the southern Dead Sea Fault System. Geochemistry, Geophysics, Geosystems 12, Q12021. http://dx.doi.org/10.1029/2011GC003736.

Amelung, F., Bell, J.W., 2003. Interferometric synthetic aperture radar observations of the 1994 Double Spring Flat, Nevada, earthquake (M 5.9): main shock accompanied by triggered slip on a conjugate fault. Journal of Geophysical Research 108.

Amoruso, A., Crescentini, L., D'Anastasio, E., De Martini, P., 2005. Clues of postseismic relaxation for the 1915 Fucino earthquake (central Italy) from modeling of leveling data. Geophysical Research Letters 32, L22307. http://dx.doi.org/10.1029/2005GL024139.

Antolik, M., Dreger, D.S., 2003. Rupture process of the 26 January 2001 Mw 7.6 Bhuj, India, earthquake from teleseismic broadband data. Bulletin of the Seismological Society of America 93, 1235–1248 (http://www.bssaonline.org/cgi/reprint/93/3/1235.pdf).

Antolik, M., Abercrombie, R.E., Ekstrom, G., 2004. The 14 November 2001 Kokoxili (Kunlunshan), Tibet, earthquake: rupture transfer through a large extensional stepover. The Bulletin of the Seismological Society of America 94, 1173–1194.

Árnadóttir, T., Jiang, W., Feigl, K.L., et al., 2006. Kinematic models of plate boundary deformation in southwest Iceland derived from GPS observations. Journal of Geophysical Research 111, B07402. http://dx.doi.org/10.1029/2005JB003907.

Árnadóttir, T., Lund, B., Jiang, W., et al., 2009. Glacial rebound and plate spreading: results from the first countrywide GPS observations in Iceland. Geophysical Journal International 177, 691–716.

Asano, K., Iwata, T., 2009. Source rupture process of the 2004 Chuetsu, Mid-Niigata Prefecture, Japan, earthquake inferred from waveform inversion with dense strong-motion data. Bulletin of the Seismological Society of America 99, 123–140.

Atzori, S., Antonioli, A., 2011. Optimal fault resolution in geodetic inversion of coseismic data. Geophysics Journal International 185, 529–538.

Audet, P., Bürgmann, R., 2011. Dominant role of tectonic inheritance in supercontinent cycles. Nature Geoscience 4, 184–187.

Avouac, J.P., Ayoub, F., Leprince, S., Konca, O., Helmberger, D.V., 2006. The 2005, M_w 7.6 Kashmir earthquake: sub-pixel correlation of ASTER images and seismic waveforms analysis. Earth and Planetary Science Letters 249, 514–528.

Baer, G., Funning, G.J., Shamir, G., Wright, T.J., 2008. The 1995 November 22, M_w 7.2 Gulf of Elat earthquake cycle revisited. Geophysics Journal International 175, 1040–1054.

Banerjee, P., Bürgmann, R., 2002. Convergence across the northwest Himalaya from GPS measurements. Geophysical Research Letters 29. http://dx.doi.org/10.1029/2002GL015184.

Banerjee, P., Bürgmann, R., Nagarajan, B., Apel, E., 2008. Intraplate deformation of the Indian subcontinent. Geophysical Research Letters 35, L09605. http://dx.doi.org/10.1029/2004GL019723.

Bassin, C., Laske, G., Masters, G., 2000. The current limits of resolution for surface wave tomography in North America. EOS. Transactions of the American Geophysical Union 81 (S12A-03).

Battaglia, M., Murray, M.H., Serpelloni, E., Bürgmann, R., 2004. The Adriatic region: an independent microplate within the Africa–Eurasia collision zone. Geophysical Research Letters 31, L18301. http://dx.doi.org/10.1029/2008GL035468.

Bayer, R., Chery, J., Tatar, M., et al., 2006. Active deformation in Zagros–Makran transition zone inferred from GPS measurements. Geophysical Journal International 165, 373–381.

Beavan, J., Moore, M.A., Pearson, C.H., et al., 1999. Crustal deformation during 1994–1998 due to oblique continental collision in the central Southern Alps, New Zealand, and implications for seismic potential of the Alpine fault. Journal of Geophysical Research 104, 25233–25255.

Beavan, J., Denys, P., Denham, M., et al., 2010. Distribution of present-day vertical deformation across the Southern Alps, New Zealand, from 10 years of GPS data. Geophysical Research Letters 37, L16305. http://dx.doi.org/10.1029/2010GL044165.

Belabbès, S., Meghraoui, M., Çakir, Z., Bouhadad, Y., 2009a. InSAR analysis of a blind thrust rupture and related active folding: the 1999 Ain Temouchent earthquake (M_w 5.7, Algeria) case study. Journal of Seismology 13, 421–432.

Belabbès, S., Wicks, C., Çakir, Z., Meghraoui, M., 2009b. Rupture parameters of the 2003 Zemmouri (M_w 6.8), Algeria, earthquake from joint inversion of interferometric synthetic aperture radar, coastal uplift, and GPS. Journal of Geophysical Research 114.

Bell, M.A., Elliott, J.R., Parsons, B.E., 2011. Interseismic strain accumulation across the Manyi fault (Tibet) prior to the 1997 Mw 7.6 earthquake. Geophysical Research Letters 38, L24302. http://dx.doi.org/10.1029/2011GL049762.

Bendick, R., Bilham, R., Freymueller, J., et al., 2000. Geodetic evidence for a low slip rate in the Altyn Tagh fault system. Nature 404, 69–72.

Benford, B., DeMets, C., Tikoff, B., et al., 2012. Seismic hazard along the southern boundary of the Gônave microplate: block modelling of GPS velocities from Jamaica and nearby islands, northern Caribbean. Geophysical Journal International 190, 59–74.

Berberian, M., Jackson, J.A., Qorashi, M., Khatib, M.M., Priestley, K., Talebian, M., Ghafuri-Ashtiani, M., 1999. The 1997 May 10 Zirkuh (Qa'enat) earthquake (M_w 7.2): faulting along the Sistan suture zone of eastern Iran. Geophysics Journal International 136, 671–694.

Berberian, M., Jackson, J.A., Qorashi, M., Talebian, M., Khatib, M., Priestley, K., 2000. The 1994 Sefidabeh earthquakes in eastern Iran: blind thrusting and bedding-plane slip on a growing anticline, and active tectonics of the Sistan suture zone. Geophysics Journal International 142, 283–299.

Berberian, M., Jackson, J.A., Fielding, E., Parsons, B.E., Priestley, K., Qorashi, M., Talebian, M., Walker, R., Wright, T.J., Baker, C., 2001. The 1998 March 14 Fandoqa earthquake (M_w 6.6) in Kerman province, southeast Iran: re-rupture of the 1981 Sirch earthquake fault, triggering of slip on adjacent thrusts and the active tectonics of the Gowk fault zone. Geophysics Journal International 146, 371–398.

Bernard, P., Briole, P., Meyer, B., Lyon-Caen, H., Gomez, J.M., Tiberi, C., Berge, C., R., C., Hatzfeld, D., Lachet, C., Lebrun, B., Deschamps, A., Courboulex, F., Larroque, C., Rigo, A., Massonnet, D., Papadimitriou, P., Kassaras, J., Diagourtas, D., Makropoulos, K., Veis, G., Papazisi, E., Mitsakaki, C., Karakostas, V., Papadimitriou, E., Papanastassiou, D., Chouliaras, M., Stavrakakis, G., 1997. The Ms = 6.2, June 15, 1995 Aigion earthquake (Greece): evidence for low angle normal faulting in the Corinth rift. Journal of Seismology 1, 131–150.

Bettinelli, P., Avouac, J.P., Flouzat, M., et al., 2006. Plate motion of India and interseismic strain in the Nepal Himalaya from GPS and DORIS measurements. Journal of Geodesy 80, 567–589.

Biggs, J., Bergman, E., Emmerson, B., Funning, G.J., Jackson, J., Parsons, B., Wright, T.J., 2006. Fault identification for buried strike-slip earthquakes using InSAR: the 1994 and 2004 Al Hoceima, Morocco earthquakes. Geophysics Journal International 166, 1347–1362.

Biggs, J., Wright, T., Lu, Z., et al., 2007. Multi-interferogram method for measuring interseismic deformation: Denali Fault, Alaska. Geophysical Journal International 170, 1165–1179.

Biggs, J., Burgmann, R., Freymueller, J., Lu, Z., Parsons, B., Ryder, I., Schmalzle, G., Wright, T., 2009. The postseismic response to the 2002 M 7.9 Denali Fault earthquake: constraints from InSAR 2003–2005. Geophysical Journal International 176, 353–367.

Biggs, J., Nissen, E., Craig, T., Jackson, J., Robinson, D.P., 2010. Breaking up the hanging wall of a rift-border fault: the 2009 Karonga earthquakes, Malawi. Geophysical Research Letters 37.

Bilham, R., Larson, K., Freymueller, J., et al., 1997. GPS measurements of present-day convergence across the Nepal Himalaya. Nature 386, 61–64.

Björnsson, A., 2008. Temperature of the Icelandic crust: inferred from electrical conductivity, temperature surface gradient, and maximum depth of earthquakes. Tectonophysics 447, 136–141.

Bruhat, L., Barbot, S., Avouac, J.P., 2011. Evidence for postseismic deformation of the lower crust following the 2004 Mw 6.0 Parkfield earthquake. Journal of Geophysical Research 116, B08401. http://dx.doi.org/10.1029/2010JB008073.

Bürgmann, R., Dresen, G., 2008. Rheology of the lower crust and upper mantle: evidence from rock mechanics, geodesy, and field observations. Annual Review of Earth and Planetary Sciences 36, 531–567.

Burgmann, R., Ayhan, M.E., Fielding, E.J., Wright, T.J., McClusky, S., Aktug, B., Demir, C., Lenk, O., Turkezer, A., 2002. Deformation during the 12 November 1999 Duzce, Turkey, earthquake, from GPS and InSAR data. Bulletin of the Seismological Society of America 92, 161–171 (http://www.bssaonline.org/cgi/reprint/92/1/161.pdf).

Bürgmann, R., Ergintav, S., Segall, P., et al., 2002. Time-dependent distributed afterslip on and deep below the Izmit earthquake rupture. Bulletin of the Seismological Society of America 92, 126–137.

Burov, E., 2010. The equivalent elastic thickness (T_e), seismicity and the long-term rheology of continental lithosphere: time to burn-out "crème brûlée": insights from large-scale geodynamic modeling. Tectonophysics 484, 4–26.

Burov, E.B., Watts, A.B., 2006. The long-term strength of continental lithosphere: 'jelly sandwich' or 'créme brûlée'? GSA Today 16, 4–10.

Cakir, Z., Akoglu, A.M., 2008. Synthetic aperture radar interferometry observations of the M = 6.0 Orta earthquake of 6 June 2000 (NW Turkey): reactivation of a listric fault. Geochemistry, Geophysics, Geosystems 9.

Çakir, Z., de Chabalier, J.B., Armijo, R., Meyer, B., Barka, A., Peltzer, G., 2003. Coseismic and early post-seismic slip associated with the 1999 Izmit earthquake (Turkey), from SAR interferometry and tectonic field observations. Geophysics Journal International 155, 93–110.

Çakir, Z., Akoglu, A.M., Belabbes, S., et al., 2005. Creeping along the Ismetpasa section of the North Anatolian fault (Western Turkey): rate and extent from InSAR. Earth and Planetary Science Letters 238, 225–234.

Calais, E., Mazabraud, Y., Mercier de Lépinay, B., et al., 2002. Strain partitioning and fault slip rates in the northeastern Caribbean from GPS measurements. Geophysical Research Letters 29, 1856. http://dx.doi.org/10.1029/2002GL015397.

Calais, E., Vergnolle, M., Sankov, V., et al., 2003. GPS measurements of crustal deformation in the Baikal–Mongolia area (1994–2002): implications for current kinematics of Asia. Journal of Geophysical Research 108 (B10), 2501. http://dx.doi.org/10.1029/2002JB002373.

Calais, E., Freed, A., Mattioli, G., Amelung, F., Jónsson, S., Jansma, P., Hong, S.H., Dixon, T., Prépetit, C., Momplaisir, R., 2010. Transpressional rupture of an unmapped fault during the 2010 Haiti earthquake. Nature Geoscience 3, 794–799.

Cavalie, O., Lasserre, C., Doin, M.P., Peltzer, G., Sun, J., Xu, X., Shen, Z.K., 2008. Measurement of interseismic strain across the Haiyuan fault (Gansu, China), by InSAR. Earth and Planetary Science Letters 275, 246–257.

Cetin, E., Meghraoui, M., Cakir, Z., et al., 2012. Seven years of postseismic deformation following the 2003 Mw = 6.8 Zemmouri earthquake (Algeria) from InSAR time series. Geophysical Research Letters 39, L10307. http://dx.doi.org/10.1029/2012GL051344.

Chen, Q., Freymueller, J.T., Yang, Z., et al., 2004. Spatially variable extension in southern Tibet based on GPS measurements. Journal of Geophysical Research 109, B09401. http://dx.doi.org/10.1029/2002JB002350.

Cirella, A., Piatanesi, A., Cocco, M., Tinti, E., Scognamiglio, L., Michelini, A., Lomax, A., Boschi, E., 2009. Rupture history of the 2009 L'Aquila (Italy) earthquake from non-linear joint inversion of strong motion and GPS data. Geophysical Research Letters 36.

Copley, A., Hollingsworth, J., Bergman, E., 2012. Constraints on fault and lithosphere rheology from the coseismic slip and postseismic afterslip of the 2006 Mw 7.0 Mozambique earthquake. Journal of Geophysical Research 117.

Crosby, A., 2007. An assessment of the accuracy of admittance and coherence estimates using synthetic data. Geophysical Journal International 171, 25–54.

D'Agostino, N., Cheloni, D., Mantenuto, S., et al., 2005. Strain accumulation in the southern Alps (NE Italy) and deformation at the northeastern boundary of Adria observed by CGPS measurements. Geophysical Research Letters 32, L19306. http://dx.doi.org/10.1029/2005GL024266.

D'Agostino, N., Mantenuto, S., D'Anastasio, E., et al., 2011. Evidence for localized active extension in the central Apennines (Italy) from global positioning system observations. Geology 39, 291–294.

D'Agostino, N., Cheloni, D., Fornaro, G., Giuliani, R., Reale, D., 2012. Space-time distribution of afterslip following the 2009 L'Aquila earthquake. Journal of Geophysical Research 117, B02402. http://dx.doi.org/10.1029/2011JB008523.

Dalla Via, G., Sabadini, R., De Natale, G., Pingue, F., 2005. Lithospheric rheology in southern Italy inferred from postseismic viscoelastic relaxation following the 1980 Irpinia earthquake. Journal of Geophysical Research 110, B06311. http://dx.doi.org/10.1029/2004JB003539.

Decriem, J., Árnadóttir, T., Hooper, A., Geirsson, H., Sigmundsson, F., Keiding, M., Ófeigsson, B.G., Hreinsdóttir, S., Einarsson, P., Lafemina, P., Bennett, R.A., 2010. The 2008 May 29 earthquake doublet in SW Iceland. Geophysics Journal International 181, 1128–1146.

Deng, J., Gurnis, M., Kanamori, H., et al., 1998. Viscoelastic flow in the lower crust after the 1992 Landers, California, Earthquake. Science 282, 1689–1693.

Deng, J., Hudnut, K., Gurnis, M., Hauksson, E., 1999. Stress loading from viscous flow in the lower crust and triggering of aftershocks following the 1994 Northridge, California, Earthquake. Geophysical Research Letters 26, 3209–3212.

Diao, F., Xiong, X., Wang, R., 2011. Mechanisms of transient postseismic deformation following the 2001 Mw 7.8 Kunlun (China) earthquake. Pure and Applied Geophysics 168, 767–779.

Dixon, T.H., Farina, F., DeMets, C., et al., 1998. Relative motion between the Caribbean and North American plates and related boundary zone deformation from a decade of GPS observations. Journal of Geophysical Research 103, 15,157–15,182.

Djamour, Y., Vernant, P., Bayer, R., et al., 2010. GPS and gravity constraints on continental deformation in the Alborz mountain range, Iran. Geophysical Journal International 183, 1287–1301.

Djamour, Y., Vernant, P., Nankali, H.R., et al., 2011. NW Iran–eastern Turkey present-day kinematics: results from the Iranian permanent GPS network. Earth and Planetary Science Letters 307, 27–34.

Donnellan, A., Parker, J.W., Peltzer, G., 2002. Combined GPS and InSAR models of postseismic deformation from the Northridge earthquake. Pure and Applied Geophysics 159, 2261–2270.

Dreger, D.S., 1994. Empirical Green's function study of the January 17, 1994 Northridge, California earthquake. Geophysical Research Letters 21, 2633–2636.

Elliott, J.R., Biggs, J., Parsons, B., et al., 2008. InSAR slip rate determination on the Altyn Tagh Fault, northern Tibet, in the presence of topographically correlated atmospheric delays. Geophysical Research Letters 35, L12309. http://dx.doi.org/10.1029/2008GL033659.

Elliott, J.L., Larsen, C.F., Freymueller, J.T., Motyka, R.J., 2010a. Tectonic block motion and glacial isostatic adjustment in southeast Alaska and adjacent Canada constrained by GPS measurements. Journal of Geophysical Research 115, B09407. http://dx.doi.org/10.1029/2009JB007139.

Elliott, J.R., Walters, R.J., England, P.C., Jackson, J.A., Li, Z., Parsons, B., 2010b. Extension on the Tibetan plateau: recent normal faulting measured by InSAR and body wave seismology. Geophysics Journal International 183, 503–535. http://dx.doi.org/10.1111/j.1365-246X.2010.04754.x.

Elliott, J.R., Parsons, B., Jackson, J.A., Shan, X., Sloan, R.A., Walker, R.T., 2011. Depth segmentation of the seismogenic continental crust: the 2008 and 2009 Qaidam earthquakes. Geophysical Research Letters 38, L06305. http://dx.doi.org/10.1029/2011GL046897.

Elliott, J.R., Nissen, E.K., England, P.C., Jackson, J.A., Lamb, S., Li, Z., Oehlers, M., Parsons, B., 2012. Slip in the 201020132011 Canterbury earthquakes, New Zealand. Journal of Geophysical Research 117, 2010–2011. http://dx.doi.org/10.1029/2011JB008868.

Elliott, J.R., Copley, A., Holley, R., Scharer, K., Parsons, B., 2013. The 2011 Mw 7.1 Van (Eastern Turkey) earthquake. Journal of Geophysical Research 118. http://dx.doi.org/10.1002/jgrb.50117.

Ergintav, S., McClusky, S., Hearn, E., et al., 2009. Seven years of postseismic deformation following the 1999, M = 7.4 and M = 7.2, Izmit–Duzce, Turkey earthquake sequence. Journal of Geophysical Research 114.

Feigl, K.L., Sergent, A., Jacq, D., 1995. Estimation of an earthquake focal mechanism from a satellite radar interferogram: application to the December 4, 1992 Landers aftershock. Geophysical Research Letters 22, 1037–1040.

Feng, W., Li, Z., Elliott, J.R., Fukushima, Y., Hoey, T., Singleton, A., Cook, R., Xu, Z., 2013. The 2011 Mw 6.8 Burma earthquake: fault constraints provided by multiple SAR techniques. Geophysics Journal International. http://dx.doi.org/10.1093/gji/ggt254 (in press).

Fialko, Y., 2004a. Evidence of fluid-filled upper crust from observations of postseismic deformation due to the 1992 Mw 7. 3 Landers earthquake. Journal of Geophysical Research 109, B03307. http://dx.doi.org/10.1029/2003JB002985.

Fialko, Y., 2004b. Probing the mechanical properties of seismically active crust with space geodesy: study of the coseismic deformation due to the 1992 M_w 7.3 Landers (southern California) earthquake. Journal of Geophysical Research 109, B03307.

Fialko, Y., 2006. Interseismic strain accumulation and the earthquake potential on the southern San Andreas fault system. Nature 441, 968–971.

Fielding, E., McKenzie, D., 2012. Lithospheric flexure in the Sichuan basin and Longmen Shan at the eastern edge of Tibet. Geophysical Research Letters 39, L09311.

Fletcher, H.J., Freymueller, J.T., 2003. New constraints on the motion of the Fairweather fault, Alaska, from GPS observations. Geophysical Research Letters 30, 1139. http://dx.doi.org/10.1029/2002GL016476.

Floyd, M., Billiris, H., Paradissis, D., Veis, G., Avallone, A., Briole, P., McClusky, S., Nocquet, J., Palamartchouk, K., Parsons, B., et al., 2010. A new velocity field for Greece: implications for the kinematics and dynamics of the Aegean. Journal of Geophysical Research 115, B10403.

Forsyth, D., 1985. Subsurface loading and estimates of the flexural rigidity of continental lithosphere. Journal of Geophysical Research 90, 12623–12632.

Franco, A., Lasserre, C., Lyon-Caen, H., et al., 2012. Fault kinematics in northern Central America and coupling along the subduction interface of the Cocos Plate, from GPS data in Chiapas (Mexico), Guatemala and El Salvador. Geophysical Journal International 189, 1223–1236.

Freed, A.M., 2007. Afterslip (and only afterslip) following the 2004 Parkfield, California, earthquake. Geophysical Research Letters 34, L06312. http://dx.doi.org/10.1029/2006GL029155.

Freed, A., Bürgmann, R., 2004. Evidence of power-law flow in the Mojave desert mantle. Nature 430, 548–551.

Freed, A., Bürgmann, R., Calais, E., Freymueller, J., Hreinsdóttir, S., 2006. Implications of deformation following the 2002 Denali, Alaska, earthquake for postseismic relaxation processes and lithospheric rheology. Journal of Geophysical Research 111, B01401.

Fujiwara, S., Rosen, P.A., Tobita, M., Murakami, M., 1998. Crustal deformation measurements using repeat-pass JERS 1 synthetic aperture radar interferometry near the Izu Peninsula, Japan. Journal of Geophysical Research 103, 2411–2426.

Fukushima, Y., Ozawa, T., Hashimoto, M., 2008. Fault model of the 2007 Noto Hanto earthquake estimated from PALSAR radar interferometry and GPS data. Earth, Planets and Space 60, 99–104.

Funning, G.J., 2005. Source Parameters of Large Shallow Earthquakes in the Alpine–Himalayan Belt From InSAR and Waveform Modelling. (Ph.D. thesis) Department of Earth Sciences, University of Oxford, Oxford, U.K.

Funning, G.J., Barke, R.M.D., Lamb, S.H., Minaya, E., Parsons, B., Wright, T.J., 2005a. The 1998 Aiquile, Bolivia earthquake: a seismically active fault revealed with InSAR. Earth and Planetary Science Letters 232, 39–49.

Funning, G.J., Parsons, B., Wright, T.J., Jackson, J.A., Fielding, E.J., 2005b. Surface displacements and source parameters of the 2003 Bam (Iran) earthquake from Envisat advanced synthetic aperture radar imagery. Journal of Geophysical Research 110, B09406.

Funning, G.J., Parsons, B., Wright, T.J., 2007. Fault slip in the 1997 Manyi, Tibet earthquake from linear elastic modelling of InSAR displacements. Geophysics Journal International 169, 988–1008.

Gan, W., Svarc, J.L., Savage, J.C., Prescott, W.H., 2000. Strain accumulation across the Eastern California Shear Zone at latitude 36° 30′N. Journal of Geophysical Research 105, 16,229–16,236.

Genrich, J., Bock, Y., McCaffrey, R., et al., 2000. Distribution of slip at the northern Sumatran fault system. Journal of Geophysical Research 105, 28327–28341.
Gomez, F., Karam, G., Khawlie, M., et al., 2007. Global Positioning System measurements of strain accumulation and slip transfer through the restraining bend along the Dead Sea fault system in Lebanon. Geophysical Journal International 168, 1021–1028.
Gourmelen, N., Amelung, F., 2005. Postseismic mantle relaxation in the central Nevada seismic belt. Science 310, 1473–1476.
Gourmelen, N., Amelung, F., Lanari, R., 2010. Interferometric synthetic aperture radar GPS integration: interseismic strain accumulation across the Hunter Mountain fault in the eastern California shear zone. Journal of Geophysical Research 115, B09408. http://dx.doi.org/10.1029/2009JB007064.
Hammond, W.C., Thatcher, W., 2007. Crustal deformation across the Sierra Nevada, northern Walker Lane, Basin and Range transition, western United States measured with GPS, 2000–004. Journal of Geophysical Research 112, B05411. http://dx.doi.org/10.1029/2006JB004625.
Hammond, W.C., Kreemer, C., Blewitt, G., 2009. Geodetic constraints on contemporary deformation in the northern Walker Lane: 3. Central Nevada seismic belt postseismic relaxation. In: Oldow, J.S., Cashman, P.H. (Eds.), Late Cenozoic Structure and Evolution of the Great Basin Sierra Nevada Transition: Geological Society of America Special Paper, pp. 33–54.
Hammond, W., Blewitt, G., Kreemer, C., 2011. Block modeling of crustal deformation of the northern Walker Lane and Basin and Range from GPS velocities. Journal of Geophysical Research 116, B04402.
Hao, K.X., Si, H., Fujiwara, H., Ozawa, T., 2009. Coseismic surface-ruptures and crustal deformations of the 2008 Wenchuan earthquake Mw 7.9, china. Geophysical Research Letters 36.
Hasterok, D., Chapman, D.S., 2008. Global heat flow: a new database and a new approach. AGU Fall Meeting Abstracts.
Hatzfeld, D., Karakostas, V., Ziazia, M., Selvaggi, G., Leborgne, S., Berge, C., Guiguet, R., Paul, A., Voidomatis, P., Diagnourtas, D., Kassaras, I., Koutsikos, I., Makropoulos, K., Azzara, R., Di Bona, M., Baccheschi, S., Bernard, P., Papaioannou, C., 1997. The Kozani–Grevena (Greece) earthquake of 13 May 1995 revisited from a detailed seismological study. Bulletin of the Seismological Society of America 87, 463–473 (http://www.bssaonline.org/cgi/reprint/87/2/463.pdf).
Hayes, G.P., Briggs, R.W., Sladen, A., Fielding, E.J., Prentice, C., Hudnut, K., Mann, P., Taylor, F.W., Crone, A.J., Gold, R., Ito, T., Simons, M., 2010. Complex rupture during the 12 January 2010 Haiti earthquake. Nature Geoscience 3, 800–805.
Hearn, E., Bürgmann, R., Reilinger, R., 2002. Dynamics of Izmit earthquake postseismic deformation and loading of the Duzce earthquake hypocenter. Bulletin of the Seismological Society of America 92, 172–193.
Hearn, E.H., McClusky, S., Ergintav, S., Reilinger, R.E., 2009. Izmit earthquake postseismic deformation and dynamics of the North Anatolian Fault Zone. Journal of Geophysical Research 114, B08405. http://dx.doi.org/10.1029/2008JB006026.
Hernandez, B., Cocco, M., Cotton, F., Stramondo, S., Scotti, O., Courboulex, F., Campillo, M., 2004. Rupture history of the 1997 Umbria–Marche (Central Italy) main shocks from the inversion of GPS, DInSAR and near field strong motion data. Annals of Geophysics 47, 1355–1376.
Hetland, E., Hager, B., 2003. Postseismic relaxation across the Central Nevada Seismic Belt. Journal of Geophysical Research 108, 2394. http://dx.doi.org/10.1029/2002JB002257.
Hetland, E., Hager, B., 2006. The effects of rheological layering on post-seismic deformation. Geophysical Journal International 166, 277–292.
Hikima, K., Koketsu, K., 2004. Source processes of the foreshock, mainshock and largest aftershock in the 2003 Miyagi-ken Hokubu, Japan, earthquake sequence. Earth, Planets and Space 56, 87–93.
Hill, E.M., Blewitt, G., 2006. Testing for fault activity at Yucca Mountain, Nevada, using independent GPS results from the BARGEN network. Geophysical Research Letters 33, L14302. http://dx.doi.org/10.1029/2006GL026140.
Hofstetter, A., Thio, H.K., Shamir, G., 2003. Source mechanism of the 22/11/1995 Gulf of Aqaba earthquake and its aftershock sequence. Journal of Seismology 7, 99–114.
Holden, C., 2011. Kinematic source model of the 22 February 2011 Mw 6.2 Christchurch earthquake using strong motion data. Seismological Research Letters 783–788.
Horikawa, H., 2001. Earthquake doublet in Kagoshima, Japan: rupture of asperities in a stress shadow. Bulletin of the Seismological Society of America 91, 112–127 (http://www.bssaonline.org/cgi/reprint/91/1/112.pdf).
Horikawa, H., 2008. Characterization of the 2007 Noto Hanto, Japan, earthquake. Earth, Planets and Space 60, 1017–1022.
Hsu, Y.J., Bechor, N., Segall, P., 2002. Rapid afterslip following the 1999 Chi-Chi, Taiwan earthquake. Geophysical Research Letters 19, 1754. http://dx.doi.org/10.1029/2002GL014967.
Huang, M.H., Hu, J.C., Ching, K.E., et al., 2009. Active deformation of Tainan tableland of southwestern Taiwan based on geodetic measurements and SAR interferometry. Tectonophysics 466, 322–334.
Ichinose, G.A., Smith, K.D., Anderson, J.G., 1998. Moment tensor solutions of the 1994 to 1996 Double Spring Flat, Nevada, earthquake sequence and implications for local tectonic models. Bulletin of the Seismological Society of America 88, 1363–1378 (http://www.bssaonline.org/cgi/reprint/88/6/1363.pdf).
Ide, S., Takeo, M., Yoshida, Y., 1996. Source process of the 1995 Kobe earthquake: determination of spatio-temporal slip distribution by Bayesian modeling. Bulletin of the Seismological Society of America 86, 547–566 (http://www.bssaonline.org/cgi/reprint/86/3/547.pdf).
Jackson, J.A., 2002. Strength of the continental lithosphere: time to abandon the jelly sandwich? GSA Today 12, 4–10.
Jackson, J., Bouchon, M., Fielding, E., Funning, G., Ghorashi, M., Hatzfeld, D., Nazari, H., Parsons, B., Priestley, K., Talebian, M., Tatar, M., Walker, R., Wright, T., 2006. Seismotectonic, rupture process, and earthquake-hazard aspects of the 2003 December 26 Bam, Iran, earthquake. Geophysics Journal International 166, 1270–1292.
Jackson, J., McKenzie, D., Priestley, K., Emmerson, B., 2008. New views on the structure and rheology of the lithosphere. Journal of the Geological Society 165, 453–465.
Ji, C., Wald, D.J., Helmberger, D.V., 2002. Source description of the 1999 Hector Mine, California, earthquake, part II: complexity of slip history. Bulletin of the Seismological Society of America 92, 1208–1226.
Johanson, I.A., Fielding, E.J., Rolandone, F., Burgmann, R., 2006. Coseismic and postseismic slip of the 2004 Parkfield earthquake from space-geodetic data. Bulletin of the Seismological Society of America 96, S269–S282 (http://www.bssaonline.org/cgi/reprint/96/4B/S269.pdf).
Johnson, K.M., Hilley, G.E., Bürgmann, R., 2007. Influence of lithosphere viscosity structure on estimates of fault slip rate in the Mojave region of the San Andreas fault system. Journal of Geophysical Research 112, B07408. http://dx.doi.org/10.1029/2006JB004842.
Johnson, K.M., Bürgmann, R., Freymueller, J.T., 2009. Coupled afterslip and viscoelastic flow following the 2002 Denali Fault, Alaska earthquake. Geophysical Journal International 176, 670–682.
Jolivet, R., Cattin, R., Chamot-Rooke, N., et al., 2008. Thin-plate modeling of interseismic deformation and asymmetry across the Altyn Tagh fault zone. Geophysical Research Letters 35, L02309. http://dx.doi.org/10.1029/2007GL031511.
Jolivet, R., Bürgmann, R., Houlié, N., 2009. Geodetic exploration of the elastic properties across and within the northern San Andreas Fault zone. Earth and Planetary Science Letters 288, 126–131.
Jones, L.E., Hough, S.E., 1995. Analysis of broadband records from the 28 June 1992 Big Bear earthquake: evidence of a multiple-event source. Bulletin of the Seismological Society of America 85, 688–704 (http://www.bssaonline.org/cgi/reprint/85/3/688.pdf).
Jónsson, S., 2008. Importance of post-seismic viscous relaxation in southern Iceland. Nature Geoscience 1, 136–139.
Jónsson, S., Segall, P., Pedersen, R., Björnsson, G., 2003. Post-earthquake ground movements correlated to pore-pressure transients. Nature 424, 179–183.
Jouanne, F., Mugnier, J.L., Gamond, J.F., Le Fort, P., Pandey, M.R., Bollinger, L., Flouzat, M., Avouac, J.P., 2004. Current shortening across the Himalayas of Nepal. Geophysical Journal International 157, 1–14.
Katsumata, K., Kasahara, M., Ichiyanagi, M., Kikuchi, M., Sen, R.S., Kim, C.U., Ivaschenko, A., Tatevossian, R., 2004. The 27 May 1995 Ms 7.6 Northern Sakhalin earthquake: an earthquake on an uncertain plate boundary. Bulletin of the Seismological Society of America 94, 117–130 (http://www.bssaonline.org/cgi/reprint/94/1/117.pdf).
Keiding, M., Árnadóttir, T., Sturkell, E., Geirsson, H., Lund, B., 2008. Strain accumulation along an oblique plate boundary: the Reykjanes Peninsula, southwest Iceland. Geophysical Journal International 172, 861–872.
Kirby, E., Harkins, N., Wang, E., et al., 2007. Slip rate gradients along the eastern Kunlun fault. Tectonics 26, TC2010. http://dx.doi.org/10.1029/2006TC002033.
Kontoes, C., Elias, P., Sykioti, O., Briole, P., Remy, D., Sachpazi, M., Veis, G., Kotsis, I., 2000. Displacement field and fault model for the September 7, 1999 Athens earthquake inferred from ERS2 satellite radar interferometry. Geophysical Research Letters 27, 3989–3992.
Koulali, A., Ouazar, D., Tahayt, A., et al., 2011. New GPS constraints on active deformation along the Africa–Iberia plate boundary. Earth and Planetary Science Letters 308, 211–217.
Kreemer, C., Holt, W., Haines, A., 2003. An integrated global model of present-day plate motions and plate boundary deformation. Geophysical Journal International 154, 8–34.
LaFemina, P.C., Dixon, T.H., Malservisi, R., Árnadóttir, T., Sturkell, E., Sigmundsson, F., Einarsson, P., 2005. Geodetic GPS measurements in south Iceland: strain accumulation and partitioning in a propagating ridge system. Journal of Geophysical Research 110, B11405. http://dx.doi.org/10.1029/2005JB003675.
Langbein, J., Borcherdt, R., Dreger, D., Fletcher, J., Hardebeck, J.L., Hellweg, M., Ji, C., Johnston, M., Murray, J.R., Nadeau, R., Rymer, M.J., Treiman, J.A., 2005. Preliminary report on the 28 September 2004, M 6.0 Parkfield, California earthquake. Seismological Research Letters 76, 10–26 (http://srl.geoscienceworld.org/cgi/reprint/76/1/10.pdf).
Larson, K.M., Rurgmann, R., Bilham, R., Freymueller, J.T., 1999. Kinematics of the India–Eurasia collision zone from GPS measurements. Journal of Geophysical Research 104, 1077–1093.
Lasserre, C., Peltzer, G., Crampé, F., Klinger, Y., Van der Woerd, J., Tapponnier, P., 2005. Coseismic deformation of the 2001 $M_w = 7.8$ Kokoxili earthquake in Tibet, measured by synthetic aperture radar interferometry. Journal of Geophysical Research 110.
Le Beon, M., Amrat, A.Q., Agnon, A., et al., 2008. Slip rate and locking depth from GPS profiles across the southern Dead Sea Transform. Journal of Geophysical Research 113, B11403. http://dx.doi.org/10.1029/2007JB005280.
Le Pichon, X., Chamot-Rooke, N., Rangin, C., et al., 2003. The North Anatolian fault in the Sea of Marmara. Journal of Geophysical Research 108, 2179. http://dx.doi.org/10.1029/2002JB001862.
Li, X., Cormier, V.F., Toksoz, M.N., 2002. Complex source process of the 17 August 1999 Izmit, Turkey, earthquake. Bulletin of the Seismological Society of America 92, 267–277 (http://www.bssaonline.org/cgi/reprint/92/1/267.pdf).
Li, Z., Feng, W., Xu, Z., Cross, P., Zhang, J., 2008. The 1998 M_w 5.7 Zhangbei–Shangyi (China) earthquake revisited: a buried thrust fault revealed with interferometric synthetic aperture radar. Geochemistry, Geophysics, Geosystems 9.
Li, Z., Elliott, J.R., Feng, W., Jackson, J.A., Parsons, B., Walters, R.J., 2011. The 2010 Mw 6.8 Yushu (Qinghai, China) earthquake: constraints provided by InSAR and body wave seismology. Journal of Geophysical Research 116. http://dx.doi.org/10.1029/2011JB008358.
Lohman, R.B., Simons, M., Savage, B., 2002. Location and mechanism of the Little Skull Mountain earthquake as constrained by satellite radar interferometry and seismic waveform modeling. Journal of Geophysical Research 107, 2118.

Louvari, E., Kiratzi, A., 2001. Source parameters of the 7 September 1999 Athens (Greece) earthquake based on teleseismic data. Journal of the Balkan Geophysical Society 4, 51–60.
Loveless, J., Meade, B., 2011. Partitioning of localized and diffuse deformation in the Tibetan Plateau from joint inversions of geologic and geodetic observations. Earth and Planetary Science Letters 303, 11–24.
Lyon-Caen, H., Barrier, E., Lasserre, C., et al., 2006. Kinematics of the North American Caribbean–Cocos plates in Central America from new GPS measurements across the Polochic–Motagua fault system. Geophysical Research Letters 33, L19309. http://dx.doi.org/10.1029/2006GL027694.
Lyons, S.N., Bock, Y., Sandwell, D.T., 2002. Creep along the Imperial Fault, southern California, from GPS measurements. Journal of Geophysical Research 107, 2249. http://dx.doi.org/10.1029/2001JB000763.
Maggi, A., Jackson, J., Mckenzie, D., Priestley, K., 2000. Earthquake focal depths, effective elastic thickness, and the strength of the continental lithosphere. Geology 28, 495–498.
Mahmoud, S., Reilinger, R., Mcclusky, S., Vernant, P., Tealeb, A., 2005. GPS evidence for northward motion of the Sinai Block: implications for E. Mediterranean tectonics. Earth and Planetary Science Letters 238, 217–224.
Mahsas, A., Lammali, K., Yelles, K., et al., 2008. Shallow afterslip following the 2003 May 21, Mw = 6.9 Boumerdes earthquake, Algeria. Geophysical Journal International 172, 155–166.
Massonnet, D., Feigl, K.L., 1995. Discrimination of geophysical phenomena in satellite radar interferograms. Geophysical Research Letters 22, 1537–1540.
Massonnet, D., Feigl, K.L., Vadon, H., Rossi, M., 1996a. Coseismic deformation field of the M = 6.7 Northridge, California earthquake of January 17, 1994 recorded by two radar satellites using interferometry. Geophysical Research Letters 23, 969–972.
Massonnet, D., Thatcher, W., Vadon, H., 1996b. Detection of postseismic fault-zone collapse following the Landers earthquake. Nature 382, 612–616.
Maurin, T., Masson, F., Rangin, C., et al., 2010. First global positioning system results in northern Myanmar: constant and localized slip rate along the Sagaing fault. Geology 38, 591–594.
Mazzotti, S., Hyndman, R., Flück, P., Smith, A.J., Schmidt, M., 2003. Distribution of the Pacific/North America motion in the Queen Charlotte Islands–S. Alaska plate boundary zone. Geophysical Research Letters 30, 1762. http://dx.doi.org/10.1029/2003GL017586.
McKenzie, D., Fairhead, D., 1997. Estimates of the effective elastic thickness of the continental lithosphere from Bouguer and free air gravity anomalies. Journal of Geophysical Research 102, 27523–27527.
McKenzie, D., Jackson, J., Priestley, K., 2005. Thermal structure of oceanic and continental lithosphere. Earth and Planetary Science Letters 233, 337–349.
Meade, B., 2007. Present-day kinematics at the India–Asia collision zone. Geology 35, 81–84.
Meade, B.J., Hager, B.H., Mcclusky, S.C., Reilinger, R.E., 2002. Estimates of seismic potential in the Marmara Sea region from block models of secular deformation constrained by Global Positioning System measurements. Bulletin of the Seismological Society of America 92, 208–215.
Meng, G., Ren, J., Wang, M., et al., 2008. Crustal deformation in western Sichuan region and implications for 12 May 2008 Ms 8.0 earthquake. Geochemistry, Geophysics, Geosystems 9, Q11007. http://dx.doi.org/10.1029/2008GC002144.
Metzger, S., Jónsson, S., Geirsson, H., 2011. Locking depth and slip-rate of the Húsavík Flatey fault, North Iceland, derived from continuous GPS data 2006–2010. Geophysical Journal International 187, 564–576.
Moore, M., England, P., Parsons, B., 2002. Relation between surface velocity field and shear wave splitting in the South Island of New Zealand. Journal of Geophysical Research 107, 2198. http://dx.doi.org/10.1029/2000JB000093.
Motagh, M., Hoffmann, J., Kampes, B., et al., 2007. Strain accumulation across the Gazikoy–Saros segment of the North Anatolian Fault inferred from Persistent Scatterer Interferometry and GPS measurements. Earth and Planetary Science Letters 255, 432–444.
Nakahara, H., Nishimura, T., Sato, H., Ohtake, M., Kinoshita, S., Hamaguchi, H., 2002. Broadband source process of the 1998 Iwate Prefecture, Japan, earthquake as revealed from inversion analyses of seismic waveforms and envelopes. Bulletin of the Seismological Society of America 92, 1708–1720.
Nakamura, T., Tsuboi, S., Kaneda, Y., Yamanaka, Y., 2010. Rupture process of the 2008 Wenchuan, China earthquake inferred from teleseismic waveform inversion and forward modeling of broadband seismic waves. Tectonophysics 491, 72–84.
Nazareth, J.J., Hauksson, E., 2004. The seismogenic thickness of the southern California crust. Bulletin of the Seismological Society of America 94, 940–960.
Nishimura, T., Thatcher, W., 2003. Rheology of the lithosphere inferred from postseismic uplift following the 1959 Hebgen Lake earthquake. Journal of Geophysical Research 108, 2389. http://dx.doi.org/10.1029/2002JB002191.
Nishimura, T., Fujiwara, S., Murakami, M., Tobita, M., Nakagawa, H., Sagiya, T., Tada, T., 2001. The M 6.1 earthquake triggered by volcanic inflation of Iwate volcano, northern Japan, observed by satellite radar interferometry. Geophysical Research Letters 28, 635–638.
Nishimura, T., Imakiire, T., Yarai, H., Ozawa, T., Murakami, M., Kaidzu, M., 2003. A preliminary fault model of the 2003 July 26, M 6.4 northern Miyagi earthquake, northeastern Japan, estimated from joint inversion of GPS, leveling, and InSAR data. Earth, Planets and Space 55, 751–757.
Nissen, E., Emmerson, B., Funning, G.J., Mistrukov, A., Parsons, B., Robinson, D.P., Rogozhin, E., Wright, T.J., 2007. Combining InSAR and seismology to study the 2003 Siberian Altai earthquakes-dextral strike-slip and anticlockwise rotations in the northern India–Eurasia collision zone. Geophysics Journal International 169, 216–232.
Nissen, E., Yamini-Fard, F., Tatar, M., Gholamzadeh, A., Bergman, E., Elliott, J.R., Jackson, J.A., Parsons, B., 2010. The vertical separation of mainshock rupture and microseismicity at Qeshm island in the Zagros fold-and-thrust belt, Iran. Earth and Planetary Science Letters 296, 181–194. http://dx.doi.org/10.1016/j.epsl.2010.04.049.
Nyst, M., Thatcher, W., 2004. New constraints on the active tectonic deformation of the Aegean. Journal of Geophysical Research 109, B11406. http://dx.doi.org/10.1029/2003JB002830.
Oglesby, D.D., Dreger, D.S., Harris, R.A., Ratchkovski, N., Hansen, R., 2004. Inverse kinematic and forward dynamic models of the 2002 Denali Fault earthquake, Alaska. Bulletin of the Seismological Society of America 94.
Okada, Y., 1985. Surface deformation due to shear and tensile faults in a half-space. Bulletin of the Seismological Society of America 75, 1135–1154.
Ozawa, S., Murakami, M., Fujiwara, S., Tobita, M., 1997. Synthetic aperture radar interferogram of the 1995 Kobe earthquake and its geodetic inversion. Geophysical Research Letters 24, 2327–2330.
Ozawa, T., Nishimura, S., Wada, Y., Ohkura, H., 2005. Coseismic deformation of the Mid Niigata prefecture earthquake in 2004 detected by RADARSAT/InSAR. Earth, Planets and Space 57, 423–428.
Parsons, B., Wright, T., Rowe, P., Andrews, J., Jackson, J., Walker, R., Khatib, M., Talebian, M., Bergman, E., Engdahl, E.R., 2006. The 1994 Sefidabeh (eastern Iran) earthquakes revisited: new evidence from satellite radar interferometry and carbonate dating about the growth of an active fold above a blind thrust fault. Geophysics Journal International 164, 202–217.
Pathier, E., Fielding, E.J., Wright, T.J., Walker, R., Parsons, B.E., Hensley, S., 2006. Displacement field and slip distribution of the 2005 Kashmir earthquake from SAR imagery. Geophysical Research Letters 33.
Pearson, C., Denys, P., Hodgkinson, K., 2000. Geodetic constraints on the kinematics of the alpine fault in the southern south island of New Zealand, using results from the Hawea–Haast GPS transect. Geophysical Research Letters 27, 1319–1322.
Pedersen, R., Sigmundsson, F., Feigl, K.L., Árnadóttir, T., 2001. Coseismic interferograms of two M_S = 6.6 earthquakes in the South Iceland Seismic Zone. Geophysical Research Letters 28, 3341–3344 (June 2000).
Peltzer, G., Rosen, P., Rogez, F., et al., 1998. Poroelastic rebound along the Landers 1992 earthquake surface rupture. Journal of Geophysical Research 103, 30131–30145.
Peltzer, G., Crampé, F., Hensley, S., et al., 2001. Transient strain accumulation and fault interaction in the Eastern California shear zone. Geology 29, 975–978.
Pérez, O., Bilham, R., Bendick, R., et al., 2001. Velocity field across the southern Caribbean plate boundary and estimates of Caribbean/South-American plate motion using GPS geodesy 1994–2000. Geophysical Research Letters 28, 2987–2990.
Pérez-Gussinyé, M., Lowry, A., Watts, A., Velicogna, I., 2004. On the recovery of effective elastic thickness using spectral methods: examples from synthetic data and from the Fennoscandian Shield. Journal of Geophysical Research 109.
Perfettini, H., Avouac, J., 2004. Postseismic relaxation driven by brittle creep: a possible mechanism to reconcile geodetic measurements and the decay rate of aftershocks, application to the Chi-Chi earthquake, Taiwan. Journal of Geophysical Research 109, B02304. http://dx.doi.org/10.1029/2003JB002488.
Perfettini, H., Avouac, J., 2007. Modeling afterslip and aftershocks following the 1992 Landers earthquake. Journal of Geophysical Research 112, B07409. http://dx.doi.org/10.1029/2006JB004399.
Peyret, M., Rolandone, F., Dominguez, S., Djamour, Y., Meyer, B., 2008. Source model for the Mw 6.1, 31 March 2006, Chalan-Chulan earthquake (Iran) from InSAR. Terra Nova 20, 126–133.
Peyret, M., Djamour, Y., Hessami, K., et al., 2009. Present-day strain distribution across the Minab–Zendan–Palami fault system from dense GPS transects. Geophysical Journal International 179, 751–762.
Pezzo, G., Tolomei, C., Atzori, S., et al., 2012. New kinematic constraints of the western Doruneh fault, northeastern Iran, from interseismic deformation analysis. Geophysical Journal International 190, 622–628.
Pollack, H.N., Hurter, S.J., Johnson, J.R., 1993. Heat flow from the earth's interior — analysis of the global data set. Reviews of Geophysics 31, 267–280.
Pollitz, F., 1992. Postseismic relaxation theory on the spherical earth. Bulletin of the Seismological Society of America 82, 422–453.
Pollitz, F., 2003. Transient rheology of the uppermost mantle beneath the Mojave Desert, California. Earth and Planetary Science Letters 215, 89–104.
Pollitz, F., 2005. Transient rheology of the upper mantle beneath central Alaska inferred from the crustal velocity field following the 2002 Denali earthquake. Journal of Geophysical Research 110, B08407. http://dx.doi.org/10.1029/2005JB003672.
Pollitz, F., Thatcher, W., 2010. On the resolution of shallow mantle viscosity structure using postearthquake relaxation data: application to the 1999 Hector Mine, California, earthquake. Journal of Geophysical Research 115, B10412. http://dx.doi.org/10.1029/2010JB007405.
Pollitz, F., Bürgmann, R., Segall, P., 1998. Joint estimation of afterslip rate and postseismic relaxation following the 1989 Loma Prieta earthquake. Journal of Geophysical Research 103, 26975–26992.
Pollitz, F.F., Peltzer, G., Bürgmann, R., 2000. Mobility of continental mantle: evidence from postseismic geodetic observations following the 1992 Landers earthquake. Journal of Geophysical Research 105, 8035–8054.
Pollitz, F., Bürgmann, R., Thatcher, W., 2012. Illumination of rheological mantle heterogeneity by the M7.2 2010 El Mayor–Cucapah earthquake. Geochemitry Geophysics Geosystems 13, Q06002. http://dx.doi.org/10.1029/2012GC004139.
Prawirodirdjo, L., Bock, Y., McCaffrey, R., et al., 1997. Geodetic observations of interseismic strain segmentation at the Sumatra subduction zone. Geophysical Research Letters 24, 2601–2604.
Priestley, K., McKenzie, D., 2006. The thermal structure of the lithosphere from shear wave velocities. Earth and Planetary Science Letters 244, 285–301.
Pritchard, M.E., Simons, M., Rosen, P.A., Hensley, S., Webb, F.H., 2002. Co-seismic slip from the 1995 July 30 M_w = 8.1 Antofagasta, Chile, earthquake as constrained by InSAR and GPS observations. Geophysics Journal International 150, 362–376.

Reilinger, R., 1986. Evidence for postseismic viscoelastic relaxation following the 1959 M = 7.5 Hebgen Lake, Montana, earthquake. Journal of Geophysical Research 91, 9488–9494.
Reilinger, R.E., Ergintav, S., Bürgmann, R., et al., 2000. Coseismic and postseismic fault slip for the 17 August 1999, M = 7.5, Izmit, Turkey earthquake. Science 289, 1519–1524.
Reilinger, R., McClusky, S., Vernant, P., et al., 2006. GPS constraints on continental deformation in the Africa–Arabia–Eurasia continental collision zone and implications for the dynamics of plate interactions. Journal of Geophysical Research 111, B05411. http://dx.doi.org/10.1029/2005JB004051.
Rigo, A., de Chabalier, J.B., Meyer, B., Armijo, R., 2004. The 1995 Kozani–Grevena (northern Greece) earthquake revisited: an improved faulting model from synthetic aperture radar interferometry. Geophysics Journal International 157, 727–736.
Riva, R., Govers, R., 2009. Relating viscosities from postseismic relaxation to a realistic viscosity structure for the lithosphere. Geophysical Journal International 176, 614–624.
Riva, R.E.M., Borghi, A., Aoudia, A., et al., 2007. Viscoelastic relaxation and long-lasting after-slip following the 1997 Umbria–Marche (Central Italy) earthquakes. Geophysical Journal International 169, 534–546.
Romanowicz, B., Dreger, D., Pasyanos, M., Uhrhammer, R., 1993. Monitoring of strain release in central and northern California using broadband data. Geophysical Research Letters 20, 1643–1646.
Rundle, J., Jackson, D., 1977. A three-dimensional viscoelastic model of a strike slip fault. Geophysical Journal of the Royal Astronomical Society 49, 575–591.
Ryder, I., Parsons, B., Wright, T., Funning, G., 2007. Post-seismic motion following the 1997 Manyi (Tibet) earthquake: InSAR observations and modelling. Geophysical Journal International 169, 1009–1027.
Ryder, I., Bürgmann, R., Sun, J., 2010. Tandem afterslip on connected fault planes following the 2008 Nima–Gaize (Tibet) earthquake. Journal of Geophysical Research 115, B03404. http://dx.doi.org/10.1029/2009JB006423.
Ryder, I., Bürgmann, R., Pollitz, F., 2011. Lower crustal relaxation beneath the Tibetan Plateau and Qaidam Basin following the 2001 Kokoxili earthquake. Geophysical Journal International 187, 613–630.
Satyabala, S.P., 2006. Coseismic ground deformation due to an intraplate earthquake using synthetic aperture radar interferometry: the M_w 6.1 Killari, India, earthquake of 29 September 1993. Journal of Geophysical Research 111, B02302.
Satyabala, S.P., Bilham, R., 2006. Surface deformation and subsurface slip of the 28 March 1999 Mw = 6.4 west Himalayan Chamoli earthquake from InSAR analysis. Geophysical Research Letters 33, L23305.
Savage, J., 1990. Equivalent strike-slip earthquake cycles in half-space and lithosphere–asthenosphere earth models. Journal of Geophysical Research 95, 4873–4879.
Savage, J., Burford, R., 1973. Geodetic determination of relative plate motion in central California. Journal of Geophysical Research 78, 832–845.
Savage, J., Prescott, W., 1978. Asthenosphere readjustment and the earthquake cycle. Journal of Geophysical Research 83, 3369–3376.
Savage, J.C., Svarc, J.L., 1997. Postseismic deformation associated with the 1992 M_w = 7.3 Landers earthquake, southern California. Journal of Geophysical Research 102, 7565–7578.
Scheiber-Enslin, S.E., LaFemina, P.C., Sturkell, E., Hooper, A.J., Webb, S.J., 2011. Geodetic investigation of plate spreading along a propagating ridge: the Eastern Volcanic Zone, Iceland. Geophysical Journal International 187, 1175–1194.
Schmidt, D.A., Bürgmann, R., 2006. InSAR constraints on the source parameters of the 2001 Bhuj earthquake. Geophysical Research Letters 33, L02315.
Scholz, C., Bilham, R., 1991. On the mechanics of earthquake afterslip. Journal of Geophysical Research 96, 8441–8452.
Searle, M.P., Elliott, J.R., Phillips, R.J., Chung, S.L., 2011. Crustal–lithospheric and continental extrusion of Tibet. Journal of the Geological Society of London 168, 633–672. http://dx.doi.org/10.1144/0016-76492010-139.
Seeber, L., Ekström, G., Jain, S.K., Murty, C.V.R., Chandak, N., Armbruster, J.G., 1996. The 1993 Killari earthquake in central India: a new fault in Mesozoic basalt flows? Journal of Geophysical Research 101, 8543–8560.
Semmane, F., Campillo, M., Cotton, F., 2005. Fault location and source process of the Boumerdes, Algeria, earthquake inferred from geodetic and strong motion data. Geophysical Research Letters 32.
Serpelloni, E., Bürgmann, R., Anzidei, M., et al., 2010. Strain accumulation across the Messina Straits and kinematics of Sicily and Calabria from GPS data and dislocation modeling. Earth and Planetary Science Letters 298, 347–360.
Shelly, D.R., Johnson, K.M., 2011. Tremor reveals stress shadowing, deep postseismic creep, and depth-dependent slip recurrence on the lower-crustal San Andreas fault near Parkfield. Geophysical Research Letters 38.
Sheu, S.Y., Shieh, C.F., 2004. Viscoelasticafterslip concurrence: a possible mechanism in the early post-seismic deformation of the Mw 7.6, 1999 Chi-Chi (Taiwan) earthquake. Geophysical Journal International 159, 1112–1124.
Sibson, R.H., 1982. Fault zone models, heat flow, and the depth distribution of earthquakes in the continental crust of the United States. Bulletin of the Seismological Society of America 72, 151–163.
Simons, M., Fialko, Y., Rivera, L., 2002. Coseismic deformation from the 1999 Mw 7.1 Hector Mine, California, earthquake as inferred from InSAR and GPS observations. Bulletin of the Seismological Society of America 92, 1390–1402 (http://www.bssaonline.org/cgi/reprint/92/4/1390.pdf).
Sloan, R.A., Jackson, J.A., McKenzie, D., Priestley, K., 2011. Earthquake depth distributions in central Asia, and their relations with lithosphere thickness, shortening and extension. Geophysics Journal International 185, 1–29.
Smith, W.H.F., Wessel, P., 1990. Gridding with continuous curvature splines in tension. Geophysics 55, 293.
Smith-Konter, B.R., Sandwell, D.T., Shearer, P., 2011. Locking depths estimated from geodesy and seismology along the San Andreas Fault System: implications for seismic moment release. Journal of Geophysical Research 116, B06401. http://dx.doi.org/10.1029/2010JB008117.
Socquet, A., Simons, W., Vigny, C., et al., 2006a. Microblock rotations and fault coupling in SE Asia triple junction (Sulawesi, Indonesia) from GPS and earthquake slip vector data. Journal of Geophysical Research 111, B08409. http://dx.doi.org/10.1029/2005JB003963.
Socquet, A., Vigny, C., Chamotrooke, N., et al., 2006b. India and Sunda plates motion and deformation along their boundary in Myanmar determined by GPS. Journal of Geophysical Research 111, B05406. http://dx.doi.org/10.1029/2005JB003877.
Soledad Velasco, M., Bennett, R.A., Johnson, R.A., et al., 2010. Subsurface fault geometries and crustal extension in the eastern Basin and Range Province, western U.S. Tectonophysics 488, 131–142.
Spinler, J.C., Bennett, R.A., Anderson, M.L., 2010. Present day strain accumulation and slip rates associated with southern San Andreas and eastern California shear zone faults. Journal of Geophysical Research 115, B11407. http://dx.doi.org/10.1029/2010JB007424.
Stramondo, S., Tesauro, M., Briole, P., Sansosti, E., Salvi, S., Lanari, R., Anzidei, M., Baldi, P., Fornaro, G., Avallone, A., Buongiorno, M.F., Franceschetti, G., Boschi, E., 1999. The September 26, 1997 Colfiorito, Italy, earthquakes: modeled coseismic surface displacement from SAR interferometry and GPS. Geophysical Research Letters 26, 883–886.
Sudhaus, H., Jónsson, S., 2011. Source model for the 1997 Zirkuh earthquake (M_W = 7.2) in Iran derived from JERS and ERS InSAR observations. Geophysics Journal International 185, 676–692.
Takeuchi, C., Fialko, Y., 2012. Dynamic models of interseismic deformation and stress transfer from plate motion to continental transform faults. Journal of Geophysical Research 117, B05403. http://dx.doi.org/10.1029/2011JB009056.
Talebian, M., Biggs, J., Bolourchi, M., Copley, A., Ghassemi, A., Ghorashi, M., Hollingsworth, J., Jackson, J., Nissen, E., Oveisi, B., Parsons, B., Priestley, K., Saiidi, A., 2006. The Dahuiyeh (Zarand) earthquake of 2005 February 22 in central Iran: reactivation of an intramountain reverse fault. Geophysics Journal International 164, 137–148.
Tatar, O., Poyraz, F., Gürsoy, H., et al., 2012. Crustal deformation and kinematics of the Eastern Part of the North Anatolian Fault Zone (Turkey) from GPS measurements. Tectonophysics 518–521, 55–62.
Taylor, M., Peltzer, G., 2006. Current slip rates on conjugate strike-slip faults in central Tibet using synthetic aperture radar interferometry. Journal of Geophysical Research 111, B12402. http://dx.doi.org/10.1029/2005JB004014.
Tesauro, M., Kaban, M., Cloetingh, S., 2012. Global strength and elastic thickness of the lithosphere. Global and Planetary Change 90–91, 51–57.
Thatcher, W., 2007. Microplate model for the present-day deformation of Tibet. Journal of Geophysical Research 112, 1–13.
Thatcher, W., England, P., 1998. Ductile shear zones beneath strike-slip faults: implications for the thermomechanics of the San Andreas fault zone. Journal of Geophysical Research 103, 891–905.
Thatcher, W., Rundle, J., 1979. A model for the earthquake cycle in underthrust zones. Journal of Geophysical Research 84, 5540–5556.
Tobita, M., Fujiwara, S., Ozawa, S., Rosen, P.A., Fielding, E.J., Werner, C.L., Murakami, M., Nakagawa, H., Nitta, K., Murakami, M., 1998. Deformation of the 1995 North Sakhalin earthquake detected by JERS-1/SAR interferometry. Earth, Planets and Space 50, 313–325.
Umutlu, N., Koketsu, K., Milkereit, C., 2004. The rupture process during the 1999 Düzce, Turkey, earthquake from joint inversion of teleseismic and strong-motion data. Tectonophysics 391, 315–324.
Utkucu, M., Alptekin, Ö., Pınar, A., 2003. A detailed source study of the Orta (Çankırı) earthquake of June 6, 2000 (MS = 6.1): an intraplate earthquake in central Anatolia. Journal of Seismology 7, 193–202.
Vaghri, A., Hearn, E., 2012. Can lateral viscosity contrasts explain asymmetric interseismic deformation around strike-slip faults? Bulletin of the Seismological Society of America 102, 490–503.
Velasco, A.A., Ammon, C.J., Beck, S.L., 2000. Broadband source modeling of the November 8, 1997, Tibet (M_w=7.5) earthquake and its tectonic implications. Journal of Geophysical Research 105, 28065–28080.
Vergnolle, M., Pollitz, F., Calais, E., et al., 2003. Constraints on the viscosity of the continental crust and mantle from gps measurements and postseismic deformation models in western Mongolia. Journal of Geophysical Research 108, 2502.
Vigny, C., Socquet, A., Rangin, C., et al., 2003. Present-day crustal deformation around Sagaing fault, Myanmar. Journal of Geophysical Research 108, 2533. http://dx.doi.org/10.1029/2002JB001999.
Wald, D.J., Heaton, T.H., 1994. Spatial and temporal distribution of slip for the 1992 Landers, California, earthquake. Bulletin of the Seismological Society of America 84, 668–691 (http://www.bssaonline.org/cgi/reprint/84/3/668.pdf).
Walker, R.T., Bergman, E.A., Elliott, J.R., Fielding, E.J., Ghods, A.R., Ghoraishi, M., Jackson, J., Nemati, M., Oviesi, B., Talebian, M., Walters, R., 2013. The 2010–2011 South Rigan (Baluchestan) earthquake sequence and its implications for distributed deformation and earthquake hazard in southeast Iran. Geophysics Journal International 193, 349–374. http://dx.doi.org/10.1093/gji/ggs109.
Wallace, K., Yin, G., Bilham, R., 2004. Inescapable slow slip on the Altyn Tagh fault. Geophysical Research Letters 31, L09613. http://dx.doi.org/10.1029/2004GL019724.
Wallace, L.M., Beavan, J., McCaffrey, R., Berryman, K., Denys, P., 2007. Balancing the plate motion budget in the South Island, New Zealand using GPS, geological and seismological data. Geophysical Journal International 168, 332–352.
Walpersdorf, A., Hatzfeld, D., Nankali, H., et al., 2006. Difference in the GPS deformation pattern of North and Central Zagros (Iran). Geophysical Journal International 167, 1077–1088.
Walters, R.J., Elliott, J.R., D'Agostino, N., England, P.C., Hunstad, I., Jackson, J.A., Parsons, B., Phillips, R., Roberts, G., 2009. The 2009 L'Aquila earthquke (Central Italy): a source

mechanism and implications for seismic hazard. Geophysical Research Letters 36. http://dx.doi.org/10.1029/2009GL039337.
Walters, R.J., Holley, R.J., Parsons, B., Wright, T.J., 2011. New signatures of underground nuclear tests revealed by satellite radar interferometry. Geophysical Research Letters 38, L05303. http://dx.doi.org/10.1029/2010GL046443.
Wang, H., Wright, T.J., 2012. Satellite geodetic imaging reveals internal deformation of western Tibet. Geophysical Research Letters 39, L07303. http://dx.doi.org/10.1029/2012GL051222.
Wang, H., Wright, T.J., Biggs, J., 2009a. Interseismic slip rate of the northwestern Xianshuihe fault from InSAR data. Geophysical Research Letters 36, L03302. http://dx.doi.org/10.1029/2008GL036560.
Wang, L., Wang, R., Roth, F., Enescu, B., Hainzl, S., Ergintav, S., 2009b. Afterslip and viscoelastic relaxation following the 1999 M 7.4 İzmit earthquake from GPS measurements. Geophysical Journal International 178, 1220–1237.
Watts, A., Zhong, S., Hunter, J., 2013. The behavior of the lithosphere on seismic to geologic timescales. Annual Review of Earth and Planetary Sciences 41.
Wdowinski, S., Bock, Y., Baer, G., et al., 2004. GPS measurements of current crustal movements along the Dead Sea Fault. Journal of Geophysical Research 109, B05403. http://dx.doi.org/10.1029/2003JB002640.
Wei, S., Fielding, E., Leprince, S., Sladen, A., Avouac, J.P., Helmberger, D., Hauksson, E., Chu, R., Simons, M., Hudnut, K., Herring, T., Briggs, R., 2011. Superficial simplicity of the 2010 El Mayor–Cucapah earthquake of Baja California in Mexico. Nature Geoscience 4, 615–618.
Wernicke, B., Davis, J.L., A, B.R., et al., 2004. Tectonic implications of a dense continuous GPS velocity field at Yucca Mountain, Nevada. Journal of Geophysical Research 109, B12404. http://dx.doi.org/10.1029/2003JB002832.
Wessel, P., Smith, W.H.F., 1998. New, improved version of generic mapping tools released. EOS Transactions AGU 79, 579.
Weston, J., Ferreira, A.M.G., Funning, G.J., 2011. Global compilation of interferometric synthetic aperture radar earthquake source models: 1. Comparisons with seismic catalogs. Journal of Geophysical Research 116.
Weston, J., Ferreira, A., Funning, G., 2012. Systematic comparisons of earthquake source models determined using InSAR and seismic data. Tectonophysics 532–535, 61–81.
Wright, T., 2002. Remote monitoring of the earthquake cycle using satellite radar interferometry. Philosophical transactions of the Royal Society of London. Series A: Mathematical Physical and Engineering Sciences 360, 2873–2888.
Wright, T.J., Parsons, B.E., Jackson, J.A., Haynes, M., Fielding, E.J., England, P.C., Clarke, P.J., 1999. Source parameters of the 1 October 1995 Dinar (Turkey) earthquake from SAR interferometry and seismic bodywave modelling. Earth and Planetary Science Letters 172, 23–37.
Wright, T., Parsons, B., Fielding, E., 2001. Measurement of interseismic strain accumulation across the North Anatolian Fault by satellite radar interferometry. Geophysical Research Letters 28, 2117–2120.
Wright, T.J., Lu, Z., Wicks, C., 2003. Source model for the M_w 6.7, 23 October 2002, Nenana Mountain earthquake (Alaska) from InSAR. Geophysical Research Letters 30.
Wright, T.J., Parsons, B., England, P.C., et al., 2004a. InSAR observations of low slip rates on the major faults of western Tibet. Science 305, 236–239.
Wright, T., Lu, Z., Wicks, C., 2004b. Constraining the slip distribution and fault geometry of the Mw 7.9, 3 November 2002, Denali fault earthquake with interferometric synthetic aperture radar and global positioning system data. Bulletin of the Seismological Society of America 94, S175–S189.
Yamasaki, T., Houseman, G.A., 2012. The signature of depth-dependent viscosity structure in post-seismic deformation. Geophysical Journal International 190, 769–784.
Yamasaki, T., Wright, T., Houseman, G., 2013. Weak ductile shear zone beneath a major strike-slip fault: inferences from earthquake cycle model constrained by geodetic observations of the western North Anatolian Fault Zone. Journal of Geophysical Research (in review).
Yang, Z., Chen, W.P., 2008. Mozambique earthquake sequence of 2006: high-angle normal faulting in southern Africa. Journal of Geophysical Research 113.
Yelles-Chaouche, A.K., Djellit, H., Beldjoudi, H., Bezzeghoud, M., Buforn, E., 2004. The Ain Temouchent (Algeria) earthquake of December 22nd, 1999. Pure and Applied Geophysics 161, 607–621.
Yu, S.B., Hsu, Y.J., Kuo, L.C., et al., 2003. GPS measurement of postseismic deformation following the 1999 Chi-Chi, Taiwan, earthquake. Journal of Geophysical Research 108, 2520. http://dx.doi.org/10.1029/2003JB002396.
Zhang, P.Z., Molnar, P., Xu, X., 2007. Late Quaternary and present-day rates of slip along the Altyn Tagh Fault, northern margin of the Tibetan Plateau. Tectonics 26, TC5010. http://dx.doi.org/10.1029/2006TC002014.